Department of Mechanical Engineering

Mechanical modeling of particulate reinforced metal matrix composites

Jairan Nafar Dastgerdi

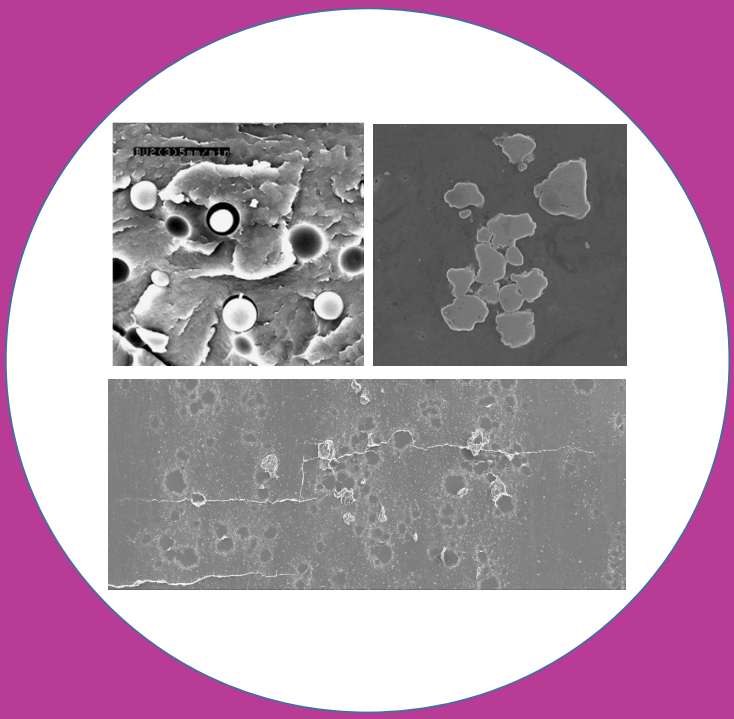

Aalto University

DOCTORAL DISSERTATIONS

Aalto University publication series
DOCTORAL DISSERTATIONS 173/2016

Mechanical modeling of particulate reinforced metal matrix composites

Jairan Nafar Dastgerdi

A doctoral dissertation completed for the degree of Doctor of Science (Technology) to be defended, with the permission of the Aalto University School of Engineering, at a public examination held at the lecture hall A of the school on 27 September 2016 at 12.

Aalto University
School of Engineering
Department of Mechanical Engineering
Mechanics of Material

Supervising professor
Prof. Gary Marquis

Preliminary examiners
Prof. Lin YE
University of Sydney
Australia

Prof. Michele Zappalorto
University of Padova
Italy

Opponents
Prof. Yukitaka Murakami
Kyushu University
Japan

Aalto University publication series
DOCTORAL DISSERTATIONS 173/2016

ISBN 978-952-60-6990-6 (printed)
ISBN 978-952-60-6989-0 (pdf)
ISSN-L 1799-4934
ISSN 1799-4934 (printed)
ISSN 1799-4942 (pdf)
http://urn.fi/URN:ISBN:978-952-60-6989-0

Unigrafia Oy
Helsinki 2016

Finland

441 697
Printed matter

Aalto University

Abstract

Aalto University, P.O. Box 11000, FI-00076 Aalto www.aalto.fi

Author
Jairan Nafar Dastgerdi

Name of the doctoral dissertation
Mechanical modeling of particulate reinforced metal matrix composites

Publisher School of Engineering

Unit Department of Mechanical Engineering

Series Aalto University publication series DOCTORAL DISSERTATIONS 173/2016

Field of research Mechanics of Material

Manuscript submitted 20 June 2016 **Date of the defence** 27 September 2016

Permission to publish granted (date) 17 August 2016 **Language** English

☐ **Monograph** ☒ **Article dissertation** ☐ **Essay dissertation**

Abstract

To predict and optimize the mechanical properties of new class of advanced composites, real engineering situations and appropriate assumptions should be considered. Moreover, a profound understanding of the relationship between real microstructure of composites and their mechanical properties is necessary. This study is concerned with the debonding damage and particle distribution effects of reinforcements on overall mechanical properties of particulate reinforced light weight metal matrix composites.

A micromechanical model is developed to take into account debonding of reinforcements, particle size and the elastoplasticity by means of incremental damage theory. Reinforcement/matrix interfacial debonding phenomena is characterized by a cohesive zone model implemented in finite element method. The results show that the assumption of fully bonded particles in composites under loading is incomplete and the influence of cohesive energy at interface is considerable. In the case of a lower cohesive energy value, there are potential sites for debonding and the stress-strain relation of damaged composite deviates from that of the perfect composite at a lower stress level.

Mechanical properties of particulate reinforced composites are highly dependent on the real microstructure of the composite and spatial distribution of reinforcement particles. A new micromechanical model based on defining clustering parameters is presented to take account of effects of the randomness of the particles. For composite with clustering defect, the clustered regions would start yielding at a higher macroscopic stress during uniaxial tension. The finite element simulation based on the real morphology shows that the plastic flow on the matrix inside the cluster is inhibited. Due to the plastic flow constraint, there is a great tendency towards debonding and crack initiation around the perimeter of a cluster. Experimental findings show that there is a strong relationship between damage formation and the local volume fraction of reinforcements.

Moreover, effects of microstructure and particle clustering on fatigue properties and crack initiation and propagation of novel amorphous particles reinforced Mg-composites are investigated. The experimental results show that the crack growth in particulate reinforced composites is a highly localized phenomenon influenced primarily by the distribution and microstructure of particles near the vicinity of the crack tip. The rate of the crack growth through the clustered region was significantly higher than through the matrix or through a region of well-dispersed particles. It is shown that composites with more uniform particle distribution possess a superior fatigue resistance and fatigue limit.

Keywords Particulate reinforced nanocomposite, Amorphous alloy reinforcments, Micromechanical modeling, Debonding, Clustering, Fatigue

ISBN (printed) 978-952-60-6990-6 **ISBN (pdf)** 978-952-60-6989-0

ISSN-L 1799-4934 **ISSN (printed)** 1799-4934 **ISSN (pdf)** 1799-4942

Location of publisher Helsinki **Location of printing** Helsinki **Year** 2016

Pages 99 **urn** http://urn.fi/URN:ISBN:978-952-60-6989-0

Acknowledgements

During the research leading to this thesis, my work has been funded by the Ministry of Education of Finland through the National Graduate program of Engineering Mechanics and the Aalto University Department of Mechanical Engineering. This financial support is gratefully acknowledged.

I would like to express my deepest gratitude to my supervisor Prof. Gary Marquis for always being supportive and eager to participate in my thesis project. Ever since, he has supported me not only by helping me to get a research assistantship but also academically and emotionally through the rough road in finishing this work. His encouragement, simulating suggestion and patience helped me during the time of research. He gave me the moral support and the freedom I needed to move on.

I would like to express my gratitude to Prof. Jukka Tuhkuri for providing a stimulating working environment for the Solid Mechanics research group. The support, scientific discussions and encouraging attitude of senior lecturer D.Sc. Kari Santoja are gratefully acknowledged.

I am grateful to my friend and colleague Susanna Hurme for her endless support, guidance, and kindness. She helped me a lot at the early stage of my arrival in Finland and during the past four years. She was the first reviewer of this thesis and her comments was really constructive and valuable.

I wish to thank the two peer reviewers of this thesis, Prof. Lin Ye from University of Sydney and Prof. Michele Zappalorto from University of Padova in Italy.

I wish to thank Prof. Yukitaka Murakami from Kyushu University in Japan for acting as my opponent.

Finally, special thanks go to my parents for their unlimited love and support. I always feel their love and positive energy even though I have been away thousands of kilometers from them for several years. My deepest and most sincere thanks go to my love, Saeed, for endless love, support, and patience during these years. I would not have been able to achieve what I have today without his belief and trust in me.

Espoo, August 29, 2016,

Jairan Nafar Dastgerdi

Contents

List of Abbreviations and Symbols

f_p, f_d	volume fractions of the intact and damaged reinforcements respectively
f_{po}	initial reinforcement volume fraction
df_p	volume fraction of the particles debonded during the incremental deformation
$d\sigma^p$	incremental stress in the intact particle
$d\sigma$, $d\bar{\sigma}$	incremental overall composite stress and the incremental average stress
L_1 , L_0	tangential moduli tensor for the particle and matrix, respectively
$d\sigma_1^{pt}, d\sigma_2^{pt}, \sigma_3^{pt}$	perturbed parts of stress
$d\varepsilon_1^{pt}, d\varepsilon_2^{pt}, \varepsilon_3^{pt}$	perturbed parts of strain
$d\varepsilon_1^*, d\varepsilon_2^*, \varepsilon_3^*$	Eshelby's equivalent transformation strain
$d\varepsilon$, $d\bar{\varepsilon}$	incremental overall composite strain and the incremental average strain
I	fourth-rank identity tensor
S	Eshelby's tensor for the spherical inclusion
σ^p	stress in the intact particle
$d\sigma_{ij}$, $d\varepsilon_{ij}$	incremental stress and strain, respectively
$d\sigma_{kk}$, $d\varepsilon_{kk}$	hydrostatic part of incremental stress and strain
$d\sigma'_{ij}, d\varepsilon'_{ij}$	deviatoric part of incremental stress and strain
κ_0 , μ_0	bulk modulus and the shear modulus of the matrix
κ_1 , μ_1	bulk modulus and the shear modulus of particles
ν_0	Poisson's ratio of the matrix
ν'_0	equivalent Poisson's ratio of the matrix in elastic-plastic deformation
μ'_0	equivalent shear modulus of the matrix in elastic-plastic deformation
H'	work-hardening ratio of the matrix
σ	normal stress at the interface
σ_{cr}	threshold bond strength between the particle and matrix
γ	specific interface adhesive energy
a	radius of particle
P	probability of debonding at the interface
S_0 , m	material parameters
$\gamma_c(\delta)$	specific interface cohesive energy

T_c	cohesive strength
δ_n , δ_t	normal and shear separation, respectively
$\overline{\delta_n}$	normal separation across the interface
V_f	total volume of particles
V_f^c	volume of particles inside a cluster
V_f^m	volume of particles in the matrix outside the cluster
V	volume of composite
V_c	volume of clusters
η	volume fraction of clusters
ζ	volume ratio of the particles inside the clusters over the total particles inside the matrix
f_1	volume fraction of particles
$\kappa_{0,eq}$, $\mu_{0,eq}$	bulk and the shear modulus of equivalent matrix, respectively
$\kappa_{1,eq}$, $\mu_{1,eq}$	bulk and the shear modulus of equivalent inclusion, respectively
$\nu_{0,eq}$	Poisson's ratio of the equivalent matrix
σ^0, σ^1	mean stress of the matrix and inclusion in the composite system, respectively
$\overline{\sigma}$	average stress based on Mori-Tanaka mean field concept
σ^{pt} , ε^{pt}	perturbed parts of stress and the response fields in reinforcements
ε_0	the strain of linearly elastic comparison material with matrix subjected to the applied stress
ε^*	Eshelby's equivalent transformation strain
σ_{kk}^0 , σ_{ij}^0	hydrostatic and deviatoric components of corresponding stresses for matrix
σ_{kk}^1 , σ_{ij}^1	hydrostatic and deviatoric components of corresponding stresses for inclusion
σ_c , σ_m	macroscopic stresses leading to start of yielding in clustered and unclustered region
σ_Y^0	ordinary tensile yield stress of the matrix

List of Publications

This doctoral dissertation consists of a summary and of the following publications which are referred to in the text by their numerals.

1. Nafar Dastgerdi, Jairan; Marquis, Gary; Salimi, Mahmoud. Micromechanical modelling of nanocomposites considering debonding of reinforcements. Composites Science and Technology, Volume 93, pages 38-45, 2014. ISSN: 0266-3538. DOI: 10.1016/j.compscitech.2013.12.020. Statu at Julkaisufoorumi is level 3.

2. Nafar Dastgerdi, Jairan; Anbarlooie, Behnam; Marzban, Saeid; Marquis, Gary. Mechanical and real microstructure behavior analysis of particulate-reinforced nanocomposite considering debonding damage based on cohesive finite element method. Composite Structures, Volume 122, Pages 518-525. 2015. ISSN: 0263-8223. DOI: 10.1016/j.compstruct.2014.12.009. Statu at Julkaisufoorumi is level 2.

3. Nafar Dastgerdi, Jairan; Marquis, Gary; Anbarlooie, Behnam; Sankaranarayanan, Seetharaman; Gupta, Manoj. Microstructure-sensitive investigation on the plastic deformation and damage initiation of amorphous particles reinforced composites. Composite Structures, Volume 142, Pages 130-139, 2016. ISSN: 0263-8223. DOI: 10.1016/j.compstruct.2016.01.075. Statu at Julkaisufoorumi is level 2.

4. Nafar Dastgerdi, Jairan; Marquis, Gary; Sankaranarayanan, Seetharaman; Gupta, Manoj. Fatigue crack growth behavior of amorphous particulate reinforced composites. Composite Structures, Volume 153, Pages 782-790, 2016. ISSN: 0263-8223. DOI: 10.1016/j.compstruct.2016.06.071. Statu at Julkaisufoorumi is level 2.

Author's Contribution

Publication 1: "Micromechanical modelling of nanocomposites considering debonding of reinforcements"

The paper presents a constitutive model of particulate-reinforced composites which can describe the debonding damage, elasto-plastic behavior of matrix and particle size effects on deformation and damage. An incremental damage model of particulate-reinforced composites based on the Mori-Tanaka's mean field concept is further developed to consider the debonding of reinforcements in nanocomposites. The author was the main author of the paper. Prof. Gary Marquis and Prof. Mahmoud Salimi contributed to the paper by giving valuable comments and suggestions.

Publication 2: "Mechanical and real microstructure behavior analysis of particulate-reinforced nanocomposite considering debonding damage based on cohesive finite element method"

This paper presents a cohesive finite element method to characterize reinforcement/matrix interface and debonding phenomena occurring, a modeling approach closely related to the real microstructure of the particulate reinforced nanocomposite. The author was the main author of the paper. Prof. Gary Marquis, Behnam Anbarlooei and Saeid Marzban contributed to the paper by giving valuable comments and suggestions.

Publication 3: "Microstructure-sensitive investigation on the plastic deformation and damage initiation of amorphous particles reinforced composites"

This paper presents a micromechanical modeling and simulation methodology based on finite element method to study effects of particle clustering on damage initiation and plastic deformation of amorphous particles reinforced composites. The paper develops an in-depth understanding of relationship between real morphology, plastic deformation and damage initiation of these novel amorphous particles reinforced composites.The author was the main author of the paper. Prof. Gary Marquis, Prof. Gupta Manoj, Behnam Anbarlooei contributed to the paper by giving valuable comments and suggestions. Seetharaman Sankaranarayanan contributed to the paper by preaparing the samples.

Publication 4: "Fatigue crack growth behavior of amorphous particulate reinforced composites"

This paper investigates the effects of microstructure and particle distribution on fatigue properties and crack growth mechanism of novel amorphous particulate reinforced composites. The author was the main author of the paper. Prof. Gary Marquis and Prof. Gupta Manoj contributed to the paper by giving valuable comments and suggestions. Seetharaman Sankaranarayanan contributed to the paper by preaparing the samples.

1. Introduction

1.1 Background

Composites are actively used in a variety of science and engineering applications such as aerospace and automotive industries. Compared with many conventional materials (such as metals, alloys, and polymers), fiber or particle reinforced composites offer prominent features such as high strength to weight ratio, high stiffness, high toughness, improved creep resistance, enhanced wear resistance, superior environmental durability, and so on. Despite such success, it has been found that the overall mechanical properties of these composites are affected by many factors such as dispersion and interfacial bonding in real engineering situations.

Theoretical predictions on effective mechanical properties of fiber or particle reinforced composites are usually made under the assumptions of high interfacial strength (with perfect bonding) and uniform distribution of inclusions. On the other hand, it is also widely recognized that the experimental mechanical properties are quite different from the theoretical expectation [Tohgo and Weng, 1994; Odegard et al., 2005, Boutaleb et al., 2009; Koyama et al., 2011, Shao et al., 2009]. It is shown that the unsatisfactory improvement in the mechanical properties of particulate-reinforced composites could be attributed to the weak bonding between particles and matrices [Nicholson, 1979; Gent, 1980; Lauke et al., 2000; Chen et al., 2010; Zappalorto et al., 2011; Lauke et al., 2013] as well as agglomeration effects of particles [Segurado et. al, 2003; Borbely et. al, 2001; Deng and Chawla 2006]. Often there is a tendency for particle clustering in the fabrication processes for real materials, so the common assumption that the particles are uniformly spaced in theoretical modeling and numerical simulation is generally more easily visualized than realized in reality. Hence, assumptions of strong or perfect interface and uniform dispersion would be inadequate for those types of composites and there is an essential demand to reliably predict and optimise the overall mechanical properties of these materials.

Moreover, mechanical properties of particulate reinforced composites are highly dependent on the real microstructure of the composite and spatial distribution of reinforcement particles. There have been some attempts in recent years to take account of effects of the randomness of the particles in the matrix [Singh et. al, 2006; Mishnaevsky et. al, 2004; Segurado and Llorca, 2006; Ayyar et. al, 2008]. It is well established experimentally that damage nucleation in polymer– and metal–matrix composites occurs in regions of the microstructure

that contain high local volume fraction of reinforcements [Lewandowski et. al, 1989; Cantwell and Roulin-Moloney, 1989]. Spatial distribution of particles determines, or at least influences significantly, several important mechanical properties such as the yield strength [Conlon and Wilkinso, 2001], the onset of damage [Li et. al, 1999; Hong et. al, 2003], the ductility [Murphy et. al, 1998], and the threshold of fatigue crack growth [Kumai et. al, 1996; Lorca 2002]. An analysis of the effect of the microstructure of materials on strength and failure mechanism of materials can be a basis for the improvement of the microstructure of materials. The optimization of the mechanical properties of composites is based on the knowledge of the relationship between the microstructure and the macroscopic response. Therefore, further understanding of the relationship between the real morphology and properties of particulate reinforced compostes is considerably important.

1.2 Objectives and scope

The objective of this thesis is to predict the mechanical properties of particulate reinforced composites based on appropriate assumptions and real engineering situations by means of analytical and computational methods. Moreover, effects of real morghology and spatial distribution of particles on mechanical properties, failure mechanism and fatigue behavior of novel lightweight metal composites reinforced with amorphous particles have been studied. To do so, the following studies have been under taken in this thesis:

- To develop an elasto-plastic incremental constitutive equation of particulate reinforced nanocomposite considering the debonding of the reinforcement and as well as the elastoplasticity using micromechanics principles.

- To characterize reinforcement/matrix interface and debonding phenomena occurring by means of a cohesive finite element method, a modeling approach closely related to the real microstructure of the particulate-reinforced nanocomposite.

- To study and understand the influence of the interfacial parameters and particle positioning on void initiation and debonding damage.

- To develop an analytical modeling to study effects of particle clustering on damage initiation and plastic deformation to advance the understanding of this defect.

- To study microstructure sensitivity of damage initiation and plastic deformation of particulate reinforced composites based on the real morphology considering the inclusions with their actual size, shape, spatial positioning, and in the exact amount using numerical simulation.

- To validate the proposed analytical and numerical simulation model through comparison with the physical experiments on the mechanical properties of novel amorphous particles reinforced Mg-composites.

- To study high cycle fatigue behavior and the ability to resist crack nucleation and propagation of $Ni_{60}Nb_{40}$/Mg composites and investigate effects of microstructure and particles distribution on fatigue properties and crack growth mechanism by *In situ* crack growth observation.

1.3 Dissertation structure

After this introductory Chapter 1, micromechanical model is developed to consider debonding of inclusions in particulate reinforced nanocomposites using incremental damage theory in Chapter 2 [Publication 1]. In Chapter 3, a cohesive finite element method is proposed to characterize reinforcement/matrix interface and debonding phenomena occurring while the real microstructure of particulate reinforced nanocomposite is considered in the modeling approach [Publication 2]. In Chapter 4, a microstructure-sensitive investigation on damage initiation and plastic deformation of amorphous particulate reinforced composites is presented considering particle clustering effects using analytical modeling and numerical simulation. In this chapter, physical experiments on mechanical properties of these new calss of composites are presented [Publication 3]. In Chapter 5, the high cycle fatigue behavior and the ability to resist crack nucleation and propagation of $Ni_{60}Nb_{40}$/Mg composites have been studied. Moreover, effects of microstructure and particle distribution on fatigue properties and crack growth mechanism are investigated [Publication 4]. Finally, concluding remarks including summary, brief discussion on the results and future work are presented in Chapter 6.

2. Simulation of debonding damage using micromechanical modeling

2.1 General marks

In composites, a variety of damage modes such as fracture of reinforcements, interfacial debonding between reinforcements and matrix, cracking in matrix, plastic yielding of voids (created by debonded inclusions) and matrix shear banding develop from the early stage of deformation under monotonic or cyclic loads. These damage modes mainly affect the mechanical performance of the composites. Therefore to extend the application of the composites and to develop even a new composite, thorough understanding of the micromechanics of damage process is essential.

In this investigation, an elasto-plastic incremental constitutive equation of particulate reinforced nanocomposite considering the debonding of the reinforcement and as well as the elastoplasticity using micromechanics principles is presented. This model is valid for the ductile matrix as metal and polymer. Shapes such as ellipsoidal (spherical, prolate and oblate) particles, elliptical and circular cylindrical fibers, disk and ribbon can be treated provided that the corresponding Eshelby tensor is used. Reinforcement damage is incorporated using Weibull approach to particle fracture and the influence of the particle size is also considered.

2.2 Theoretical modelling

2.2.1 Incremental damage theory

In Fig. 2.1, the states before and after incremental deformation of the composite in the damage process are depicted. The state before incremental deformation shown in Fig. 2.1a is described in terms of the volume fractions of the intact and damaged reinforcements, f_p and f_d. If the volume fraction of the particles that are debonded during the incremental deformation is denoted by df_p, then the state after deformation, shown in Fig. 2.1b, can be described in terms of the volume fractions of the intact and debonded particles $f_p - df_p$ and $f_d + df_p$.

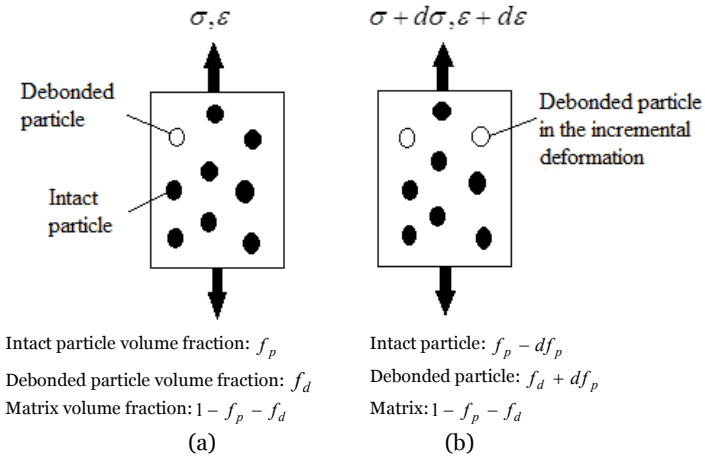

Figure 2.1. Debonding of inclusions in the deformation process: (a) before incremental deformation, (b) after incremental deformation

Eshelby's equivalence principle [Eshelby, 1957] is combined with Mori-Tanaka's mean field concept [Mori and Tanaka, 1973] to describe the deformation and damage of the composite in the incremental process. The incremental stress in the particle, $d\sigma^p$, is given by

$$\begin{aligned} d\sigma^p &= d\sigma + d\bar{\sigma} + d\sigma_1^{pt} \\ &= L_1(d\varepsilon_0 + d\bar{\varepsilon} + d\varepsilon_1^{pt}) = L_0(d\varepsilon_0 + d\bar{\varepsilon} + d\varepsilon_1^{pt} - d\varepsilon_1^*) \end{aligned} \tag{2-1}$$

where the subscript 0 refers to the matrix and 1 refers to the inclusions.

The completely debonded particles which have lost their load-carrying capacity act effectively as voids; thus, the Eshelby equivalence principle for the debonded reinforcement can be written as follows:

$$0 = d\sigma + d\bar{\sigma} + d\sigma_2^{pt} = L_0(d\varepsilon_0 + d\bar{\varepsilon} + d\varepsilon_2^{pt} - d\varepsilon_2^*) \tag{2-2}$$

Furthermore, since in the debonding process the current reinforcement stress are released in the next incremental deformation, the following equation is obtained:

$$-\sigma^p = d\sigma + d\bar{\sigma} + \sigma_3^{pt} = L_0(d\varepsilon_0 + d\bar{\varepsilon} + \varepsilon_3^{pt} - \varepsilon_3^*) \tag{2-3}$$

In the above equations, L_1 and L_0 are tangential moduli tensor for the particle and matrix, respectively. $d\sigma$ and $d\bar{\sigma}$ are the incremental overall composite stress and the incremental average stress based on Mori and Tanaka's mean field concept. $d\sigma_1^{pt}, d\sigma_2^{pt}, \sigma_3^{pt}$ and $d\varepsilon_1^{pt}, d\varepsilon_2^{pt}, \varepsilon_3^{pt}$ represent the perturbed parts of stress and the response fields in the intact and debonded reinforcements and the reinforcement to be debonded, respectively. $d\varepsilon_1^*, d\varepsilon_2^*, \varepsilon_3^*$ are Eshelby's

equivalent transformation strain. Subsequently the incremental strain $d\varepsilon$-stress $d\sigma$ relation of the composite is obtained as a function of incremental applied stress $d\sigma$ and volume fraction of the particles debonded during the incremental deformation df_p [for details, see Publication 1].

$$\begin{aligned} d\varepsilon = &\left\{(I+D_1)-[D_1(S-I)-I]H^{-1}df_p[(S-I)D_1-I]\right\}L_0^{-1}d\sigma \\ &+[D_1(S-I)-I]H^{-1}L_0^{-1}\sigma^p df_p \end{aligned} \tag{2.4}$$

where I is the fourth-rank identity tensor and S denotes Eshelby's tensor for the spherical inclusion. σ^p is the average stress of the intact inclusion and L_0 is tangential moduli tensor matrix. D_1 and H are defined based on mathematical manuplations and expressed in Publication 1.

The above equation shows that the incremental macroscopic strain of the composite consists of two parts: the strain increment due to the stress increment, and the debonding damage. Thus, Eq. (2.4) can be rewritten as follows

$$\begin{aligned} &d\varepsilon = L^{-1}d\sigma + Ddf_p \\ &L^{-1} = \left\{(I+D_1)-[D_1(S-I)-I]H^{-1}df_p[(S-I)D_1-I]\right\}L_0^{-1} \\ &D = [D_1(S-I)-I]H^{-1}L_0^{-1}\sigma^p \end{aligned} \tag{2.5}$$

2.2.2 Properties of particle and matrix

In the composite medium, the matrix undergoes elastic-plastic deformation and the reinforcement deforms elastically. The elastic incremental stress-strain relation of the particle is given in isotropic form by

$$d\varepsilon_{kk} = \frac{1}{3\kappa_1}d\sigma_{kk},\ \ d\varepsilon'_{ij} = \frac{1}{2\mu_1}d\sigma'_{ij} \tag{2.6}$$

where κ_1 and μ_1 are the bulk modulus and the shear modulus of particles. The elastic-plastic deformation of matrix is described by the Prandtl-Reuss equation [for details, see Publication 1]. The equivalent shear modulus μ'_0 and Poisson's ratio ν'_0 in elastic-plastic deformation are approximated as below [Mura, 1987]

$$\mu'_0 = \frac{\mu_0}{1+\dfrac{3\mu_0}{H'}},\quad \nu'_0 = \frac{\nu_0+\dfrac{\mu_0}{H'}(1+\nu_0)}{1+2\dfrac{\mu_0}{H'}(1+\nu_0)} \tag{2.7}$$

where H' is the work-hardening ratio of the matrix and κ_0 and μ_0 are the bulk modulus and the shear modulus of the matrix in elastic state, respectively. When matrix is in the alstio-plastic state, μ_0 and ν_0 in all equations reduce to their elastic plastic counterparts, μ'_0 and ν'_0.

Therefore, the incremental stress-strain relation of the matrix in elastic-plastic state is given by

$$d\varepsilon_{kk} = \frac{1}{3\kappa_o} d\sigma_{kk}, \quad d\varepsilon'_{ij} = \frac{1}{2\mu'_o} d\sigma'_{ij} \tag{2.8}$$

2.2.3 Cumulative probability of damaged particles

The particle encounters debonding damage when the normal stress σ at the interface reaches the threshold bond strength σ_{cr} between the particle and matrix material. A critical energy criterion for particle-matrix interfacial debonding is applied to control debonding damage and σ_{cr} is defined as below, considering particle size effect [for details, see Publication 1].

$$\sigma_{cr} = \sqrt{\frac{\gamma}{a} \frac{4E_o}{1+\nu_o}} \tag{2.9}$$

where E_o and ν_o are the initial modulus and Poisson's ratio of the matrix, respectively. γ is the specific interface adhesive energy and a is the radius of the particle. Recently other authors have reconsidered this problem, showing that for nanosized reinforcement's surface and interface effects around nanofillers might play an important role on the assessment of the critical detachment strength [Salviot et al., 2013]. They proposed a more precise formulation that can consider the interfacial effects of nanoparticles in the matrix. In the case of microparticles, or for materials where interfacial effects such as surface stresses and interphase effects are negligible, the improved equation provided by Salviato et al. exactly matches Eq.(2.9).

Assume that the probability of debonding at the interface, P, can be described using Weibull's distribution function:

$$P = 1 - \exp\left[-\left(\frac{\sigma - \sigma_{cr}}{S_o}\right)^m\right], \ (\sigma \geq \sigma_{cr}) \tag{2.10}$$

where S_o and m are material parameters and σ is the average normal stress at the interface [Lauke, 2013]. If the initial particle volume fraction is denoted by f_{po}, then the cumulative volume fraction of the damaged particles is represented by $f_{po}P$ for $\sigma_{cr} \geq \sigma$. Consequently, the volume fraction df_p of the particles debonded in the incremental deformation is given by

$$df_p = f_{po} \frac{dP}{d\sigma} d\sigma \tag{2.11}$$

2.3. Results and discussion

The applicability of the proposed theory is investigated for nanocomposites consisting of Al_2O_3 nanoparticles embedded in magnesium alloy AZ31 matrix.

Using the proposed method, the stress-strain response of the $AZ31/Al_2O_3$ nanocomposite under uniaxial tension is shown in Fig.2.2. In this figure, it can be seen that there is a large discrepancy between the perfect composite and the experimental data [Paramsothy et.al, 2012]. This discrepancy indicates that the assumption of fully bonded particles in nanocomposites under loading is incomplete. It is observed that this large discrepancy is decreased significantly when the effects of the debonding and size effect of particles on damage process are considered using the proposed method. When the debonding damage starts to occur and the volume fraction of debonded particles increases, the stress-strain curve for the damaged nanocomposite deviate to lower stress from those of the perfect one.

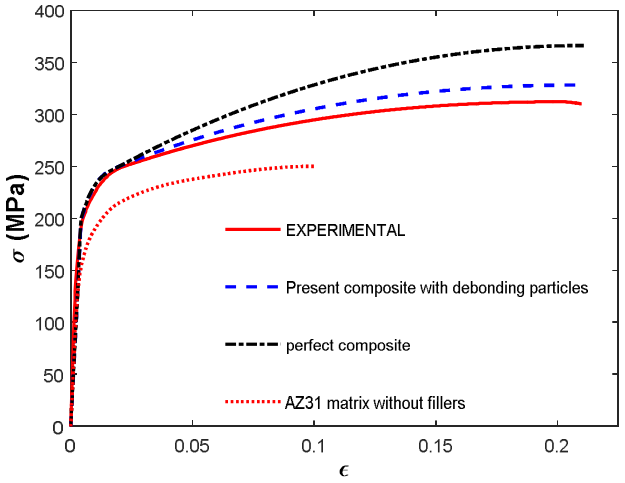

Figure 2.2. The stress-strain response of the nanocomposite under uniaxial tension

The effect of adhesive energy at interface, γ , on the stress-strain response and interfacial debonding process between the particles and the matrix is depicted in Fig. 2.3. As shown in this figure, the influence of adhesive energy at interface is considerable on the stress-strain curve. In the case of a lower γ value, the stress-strain relation of damaged composite deviate from that of the perfect composite at a lower stress level. In fact, by increasing γ, the interfacial debonding would become more difficult to occur and there is a threshold value for γ that if the adhesive energy at interface is larger than this critical value, the debonding between particles and matrix does not occur.

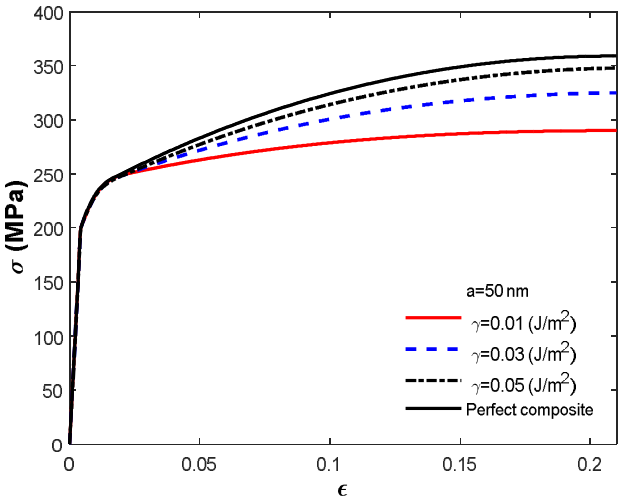

Figure 2.3. The effect of adhesive energy at interface, γ, on the stress-strain response and interfacial debonding process

The effect of particle size, a, on the stress-strain response and interfacial debonding process between the particles and the matrix is plotted in Fig. 2.4. It can be seen that the interfacial debonding between the particles and the matrix is less than that of the nanocomposites filled with particles of smaller size.

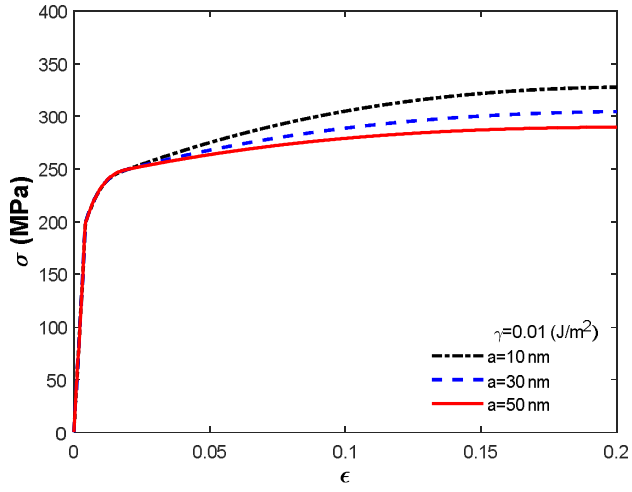

Figure 2.4. The effect of particle size, a, on the stress-strain response and interfacial debonding process

The effects of adhesive energy at interface, γ, and particle size, a, on the volume fraction of perfectly bonded and debonded particles in the nanocomposite are depicted simultaneously in Fig. 2.5. It can be seen that when the particle size decreases and the adhesive energy at interface increases, the volume fraction of perfectly bonded particles increases and the volume fraction of debonded particles decreases.

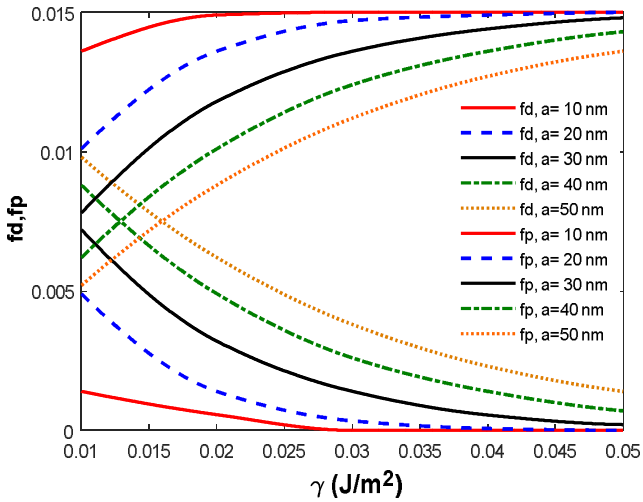

Figure 2.5. The effects of adhesive energy at interface, γ , and particle size, a , on the volume fraction of perfectly bonded and debonded particles.

3. Characterization of debonding damage using cohesive zone modelling

3.1 General marks

To gain a deeper understanding into the mechanical performance of particulate-reinforced nanocomposites and into debonding phenomena occurring, a modelling approach closely related to the real microstructure of nanocomposites is proposed. It is worth noting that FEM-based models are often applied to the so called representative volume element (RVE), thus assuming that the microstructure of the composite can be reproduced by assembling a large number of such elements. However, this can be a serious limitation when dealing with complex and highly heterogeneous composites microstructures, such as randomly dispersed particulate systems. Therefore, an approach able to consider the actual microstructure of the nanocomposite is useful in order to accurately predict the overall properties.

In this study, the cohesive zone model (CZM) has been adopted to capture the nanofillers deboning. A CZM assumes a relation between the normal (and shear traction(s) and the opening (and sliding) displacement(s). When implemented in the finite element method (FEM), the CZM is capable of simulating interface debonding and sliding.

3.2 Microstructural modeling

Typical RVE extracted from the real transmissionelectron microscope (TEM) microstructure (Fig. 3.1a) with finite element mesh is shown in Fig. 3.1b. The meshing here is a free mesh type to achieve an acceptable accuracy in the interfaces between the inclusions and matrix.

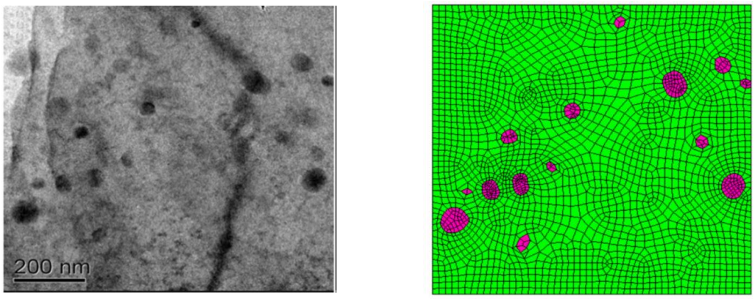

(a) (b)

Figure 3.1. (a) real TEM microstructure image [Paramsothy et.al, 2012] and (b) RVE and meshing that are used for finite element modeling

In the CZM, the damage-debonding process zone is simplified as being an initially zero-thickness zone, composed of two coinciding cohesive surfaces. Under loading, the two surfaces separate and the traction between them varies in accordance with a specified traction–separation law. The interface element constitutive model which is used in present work is the exponential softening law [Needleman and Xu, 1994] as follows:

$$\gamma_c(\delta) = \mathrm{e}\mathrm{T}_c\,\bar{\delta}_n[1-(1+\Delta_n)\mathrm{e}^{-\Delta_n}\mathrm{e}^{-\Delta_t^2}] \tag{3.1}$$

where, $\gamma_c(\delta)$ is the specific interface cohesive energy, e = 2.7182, T_c is the cohesive strength, $\Delta_n = \delta_n / \bar{\delta}_n$, and $\Delta_t = \delta_t / \bar{\delta}_t$. δ_n, δ_t are respectively normal and shear separation and $\bar{\delta}_n$ is the normal separation across the interface where the maximum normal traction is attained with $\delta_t = 0$, $\bar{\delta}_t$ is the shear separation where the maximum shear traction is attained at $\delta_t = \bar{\delta}_t\sqrt{2}/2$. The cohesive traction-separation relation is plotted in Fig. 3.2. The parameters adopted in the following simulations are $T_c = 163.27\,MPa$, $\Delta_n = 3.053\overset{o}{A}$, and $\Delta_t = 2\Delta_n$. T_c is calculated based on Eq. (2.9) and the specific interface adhesive energy, $\gamma_c = 0.005\,J/\mathrm{m}^2$. The adhesive energy can be evaluated by considering the area under the traction-separation curve and then the normal separation can be calculated as $\Delta_n = 2\gamma_c / T_c$. Since debonding process is a mixed-mode crack growth process, Δ_t is calculated using maximum shear stress criterion.

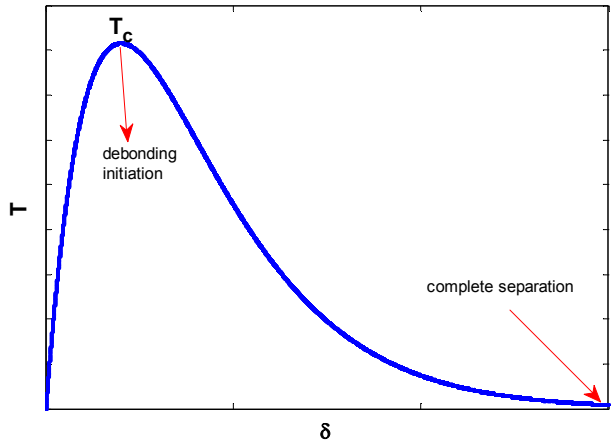

Figure 3.2. Traction-separation law for modeling cohesive failure

Moreover, the effect of mesh size in 2D RVE stress-strain curve is depicted in Fig. 3.3. The predicted stress-strain behaviors with different mesh resolutions are compared with the experimental results in this figure. The used numbers of the elements in the models were 2500 and 4500 and 7500. In both coarse and fine meshing condition RVE simulated stress-strain curve are almost same up to maximum tensile stress (i.e. instability) and slightly alters after instability point.

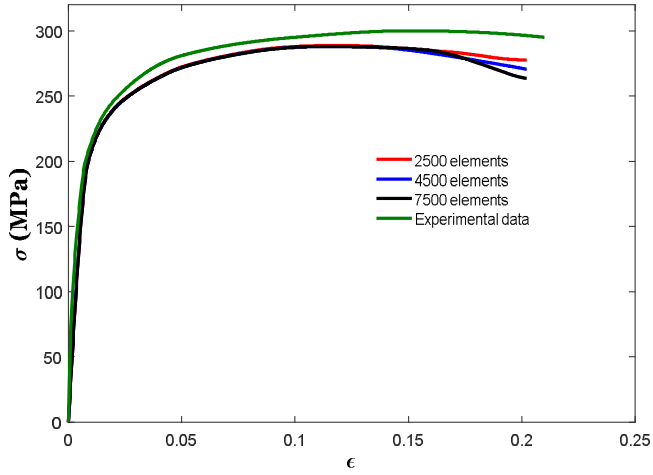

Figure 3.3. Comparison of predicted stress-strain behavior from different meshes with experimental results

3.3 Results and discussion

The stress-strain response of the $AZ31/Al_2O_3$ nanocomposite under uniaxial tension is shown in Fig. 3.4. It can be seen that there is a large discrepancy between the composite with fully bonded particles assumption and the experimental data [Paramsothy et.al, 2012]. It is observed that this large discrepancy is decreased when the effect of the debonding on damage process is considered using the present cohesive FEM. When the debonding damage starts to occur, the stress-strain curve for the damaged nanocomposite deviate to lower stress from those of the perfect one.

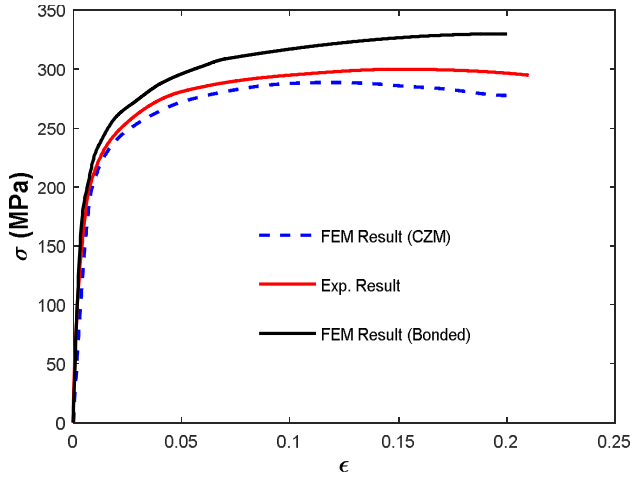

Figure 3.4. The stress-strain response of the nanocomposite under uniaxial tension

The void initiation and growth or decohesion between the reinforcements and matrix takes place at higher strained region. Therefore, strain localization zone (shear band) can be considered as a zone which is highly potential sites for void initiation. Fig. 3.5a depicts the equivalent plastic strain and multiple bands with high equivalent plastic strain are predicted within the RVE. The shear strain concentration is another indicator of void initiation in simulation. Fig. 3.5b shows the shear strain and Fig. 3.5c shows the hydrostatic stress concentration. It can be observed at the points of shear strain concentration (shown by circle in Fig. 3.5b) the internal pressure is negative. Negative internal pressure in tensile loading is an indicator of void initiation. It has to be mentioned the shear localization and hydrostatic stress concentration do not happen necessarily at the same location. There is also another point of localization (shown by an arrow in Fig. 3.5b) which acts like a potential site for debonding and then void initiation while internal pressure is not negative. In fact, this particle site is located in the joint of shear bands together (Fig. 3.5a); however, the hydrostatic stress concentration in this site is not negative. Fig. 3.5d shows the CZM normal separation of inclusions from the matrix. This figure shows how voids initiate and which zones are potential sites for debonding. It should be noted that this analysis is 2D and multiple bands with high equivalent plastic strain are predicted within the this RVE along the maximum shear direction while the effect of the

RVE morphology on process of debonding and subsequent shear banding might change in a 3D framework.

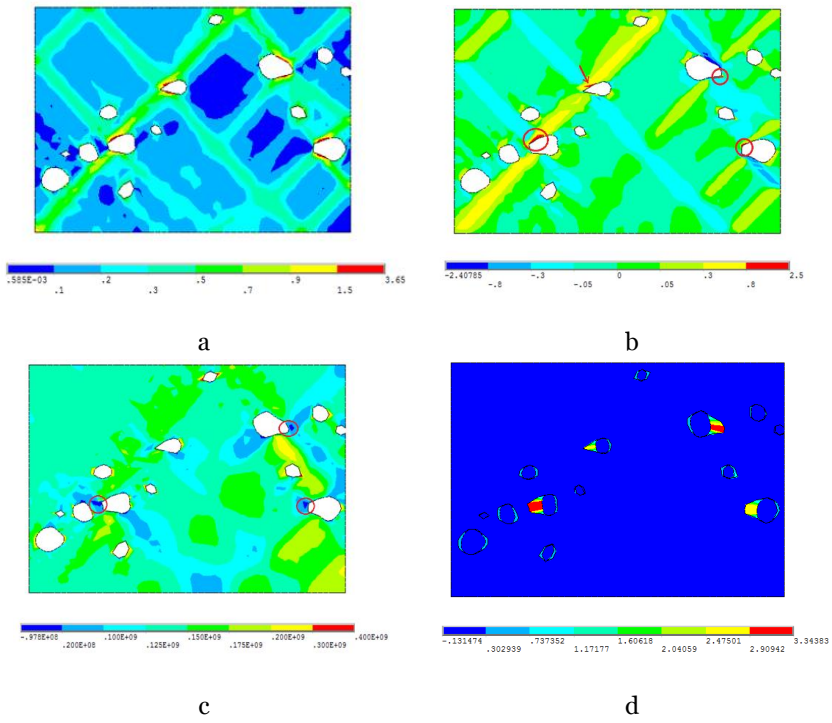

Figure 3.5. Distribution of (a) equivalent plastic strain, (b) shear plastic deformation, (c) hydrostatic pressure [MPa] and (d) CZM normal separation [A°]

The stress-strain response of the RVE under uniaxial tension is shown in Fig. 3.6 with two different kinds of modeling based on the real microstructure and array distribution of the same size spherical nanoparticles in the matrix. It can be seen that in the real microstructure modelling, there is a stationary point ($d\sigma / d\varepsilon = 0$) in $\varepsilon = 0.125$ that shows the shear instability while there is no stationary point in the array distribution modeling and the stress-strain curve is increasing. In the real microstructure modeling, it is evident the stress-strain curve can be divided into three stages according to the slope value: elastic region (stage I) where the strain is less than 0.01, stage II where the slope of the curve decreases gradually because of the weakening of the interface and reaches zero value at an ultimate strain of 12.5%, and stage III where the stress on the composite decline in a certain level owing to the fracture at the interface. In fact, after the stationary point the load carrying capacity decreases with increasing strain. This will lead to localization of strain which will tend to concentrate. It is evident that the shear bands formation is totally different in these two models. This figure shows the array distribution modelling does not accurately predict the mechanical and damage behavior of the nanocomposite.

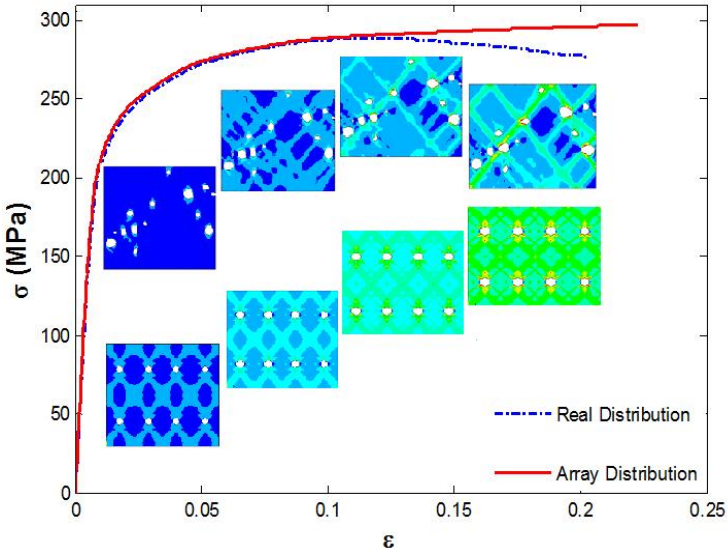

Figure 3.6. The stress-strain response of the nanocomposite under uniaxial tension with two different kinds of modelling based on the real microstructure and array distribution

4. Theoretical modelling and simulation of particle clustering

4.1 General marks

Mechanical properties of particulate reinforced composites are highly dependent on the real microstructure of the composite and particle distribution and volume fraction.The composites are often fabricated by a powder metallurgy and extrusion process or by liquid infiltration. In practice, it is often difficult to obtain a uniform and homogeneous distribution of reinforcement particles. Hence, an analysis of the effect of the microstructure of composites on the strength and failure mechanism can be a basis for the improvement of the microstructure of the composite and optimization of the mechanical properties.

In this investigation, micromechanical modelling and finite element methodology have been employed to obtain insight into particle distribution effects on mechanical properties and damage initiation of particulate reinforced composites. Analytical expressions are derived for macroscopic stress for initial yielding of the matrix with taking into account the effects of particle clustering. Simulation methodology discusses clustering based on real morphology and not based on randomly generated artificial microstructure.

4.2 Material and experimental details

Amorphous alloy powder with composition $Ni_{60}Nb_{40}$ (at. %) was prepared by mechanically alloying powder mixtures of elemental Ni and Nb metals. The powder mixture was milled at room temperature in air for 87 h, using a Retsch PM400 planetary ball mill with a ball-to-powder ratio of 3:1 and milling speed of 200 rpm. To produce Mg-composites, elemental Mg-powder (99.6% purity) was blended with varying volume fractions of $Ni_{60}Nb_{40}$ powder for a duration of 1 h and consolidated at room temperature at 450 MPa for 1 min. The compacted cylindrical billets of 36 mm diameter were microwave sintered at 100% power level for 12.30 min so as to achieve a temperature of 550^{o}C (based on prior calibration). The sintered billets were soaked at 400^{o}C for 1 h, and hot extruded at 350^{o}C to produce rods of 8 mm diameter. The extruded rods were used for further testing.

For more analytical and numerical simulation in the next sections, mechanical properties of amorphous alloy powder manufactured should be determined.

Thus, a clearly polished composite sample was scanned with atomic force microscope (AFM) probe to obtaine images of the surface topography and measure Young's modulus of $Ni_{60}Nb_{40}$ particles embedded in the matrix. Figure 4.1 shows representative images of the sample and modulus map through the cross sectional lines identified in the image with white line.

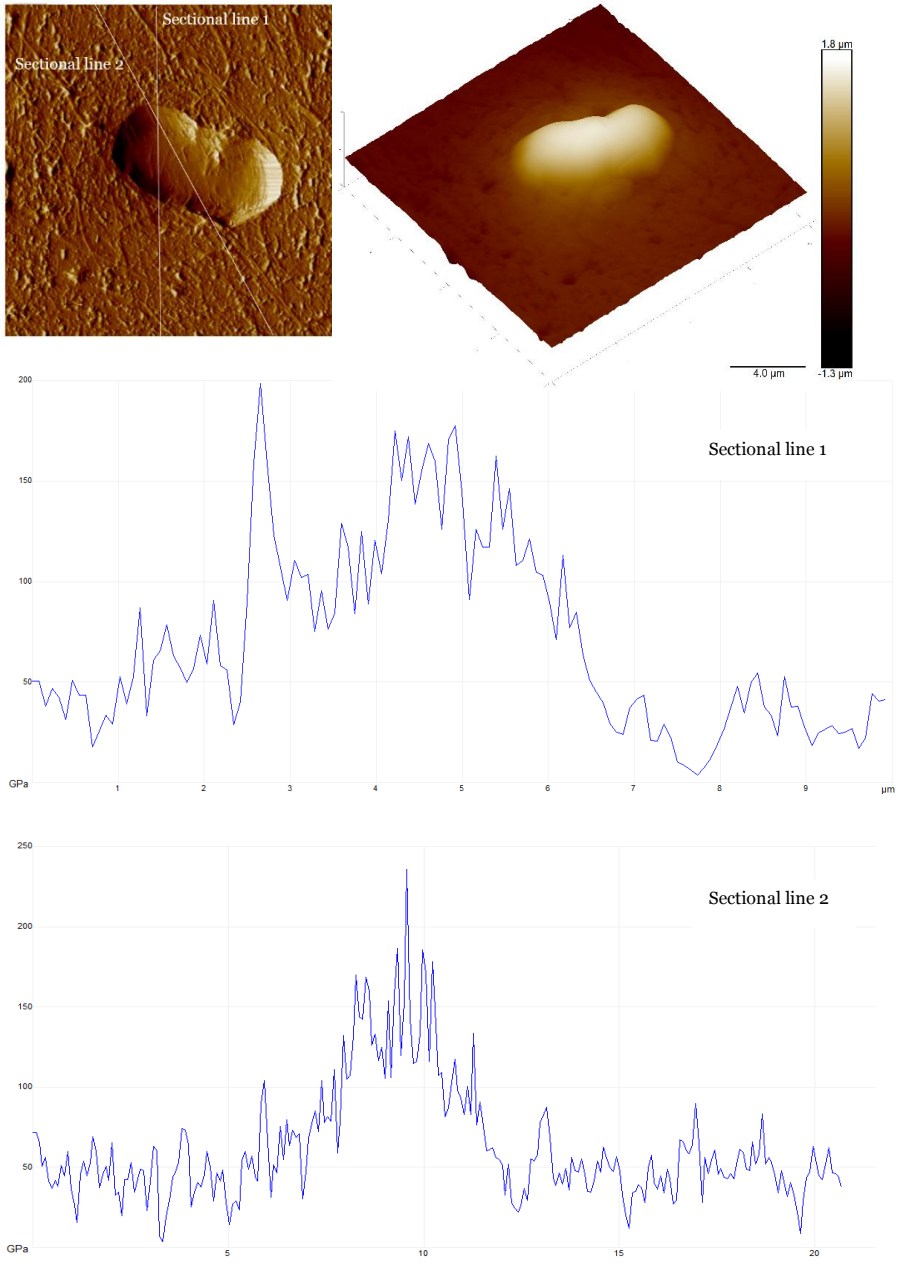

Figure 4.1. Tomographic image of the sample surface and modulus maps through cross sectional lines

The material properties of the composite constituents are presented in Table 1, based on the nanoindentation measurement.

Table 1. Material parameter of the composite constituents

Material	$E(GPa)$	ν	$\sigma_{YS}(MPa)$
Pure Mg	42.2 ± 0.9	0.35	80 ± 9
$Ni_{60}Nb_{40}$	150 ± 7	0.3	---

The microstructure of 5 vol. % $Ni_{60}Nb_{40}$/Mg composites is shown in Fig. 4. 2a. It is observed that some local regions have a higher concentration of particles than the average volume fraction in the material as depicted in Fig. 4.2c and they are considered as clusters.

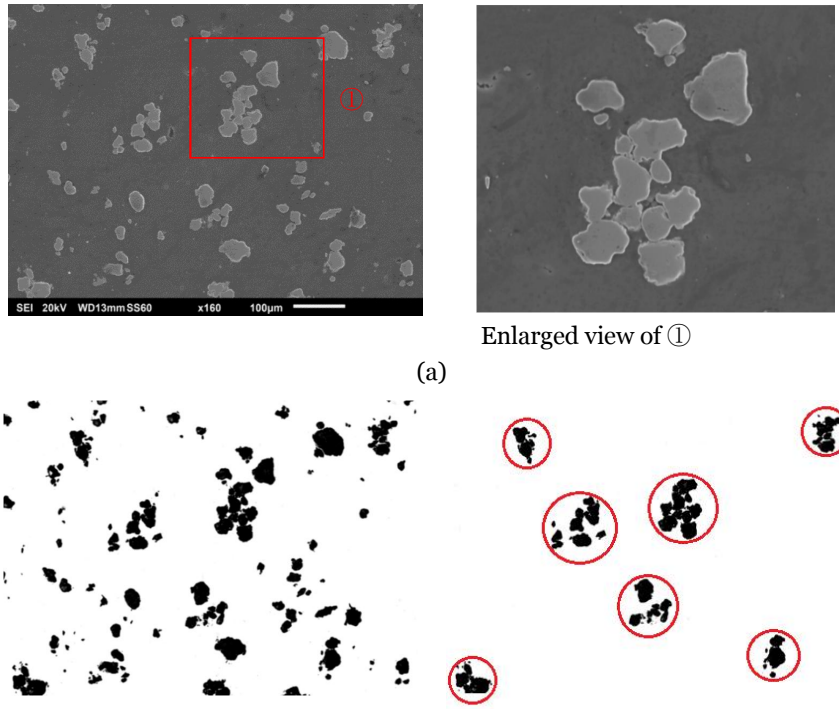

Figure 4.2. Selected RVE from real microstructure: (a) SEM image, (b) binarised microstructure, and (c) spherical regions with internal inhomogeneous distribution.

Figures 4.3a shows the fracture surface observations and stress-strain curve of the specimen chosen from billet extruded at 600 psi and Fig. 4.3b shows the transverse cross-section observations of the fractured specimen. Same observations are depicted for another specimen chosen from billet extruded at 750 psi in Fig. 4.4a-b. The transverse cross-section observations of the fractured specimens indicate the concentration of damage in the region of particle cluster. The damage nucleation occurs in regions of the microstructure that contain high local volume fraction of reinforcements.

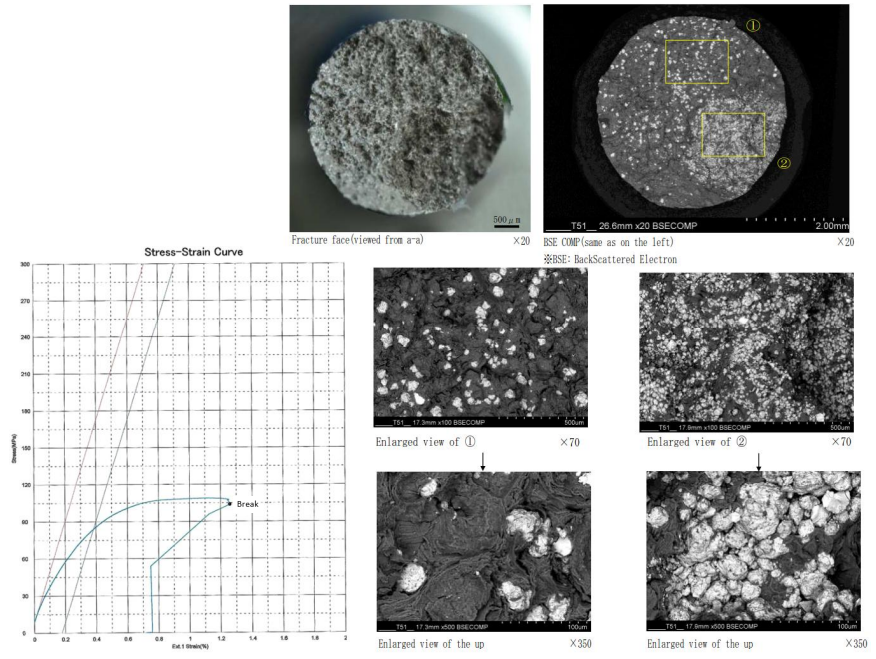

(a)

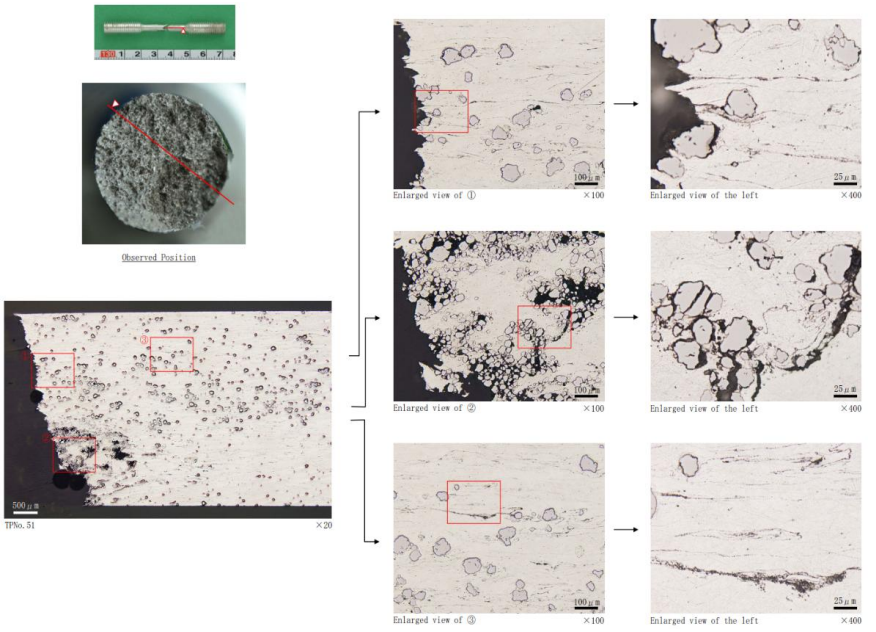

(b)

Figure 4.3. (a) Fracture surface observations, (b) the transverse cross-section observations of 5 vol. % $Ni_{60}Nb_{40}$/Mg composite (extrusion pressure 600 Psi).

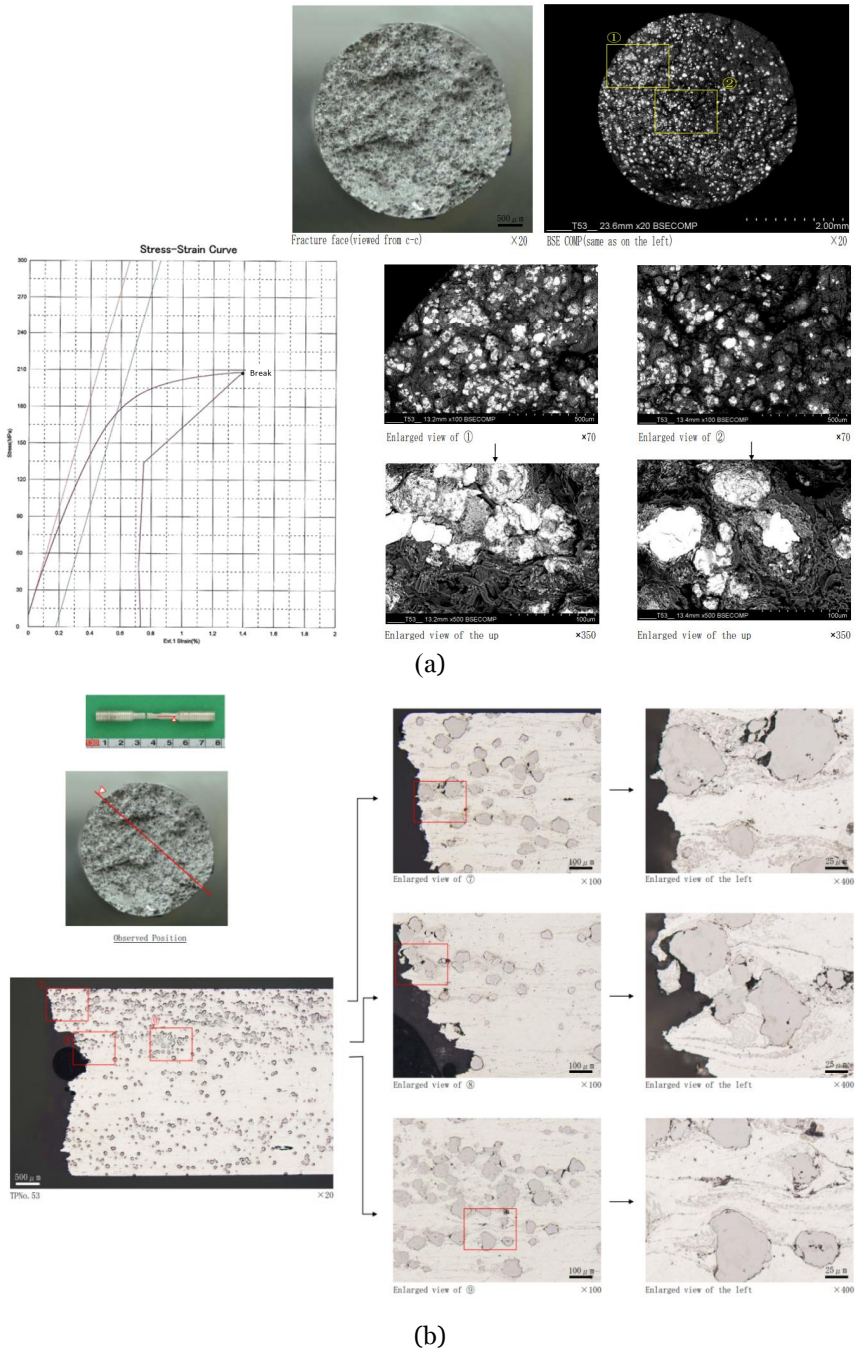

Figure 4.4. (a) Fracture surface observations, (b) the transverse cross-section observations of 5 vol. % $Ni_{60}Nb_{40}$/Mg composite (extrusion pressure 750 Psi).

Experimental findings show that there is a strong relationship between damage formation and the local volume fraction of the reinforcement. Hence the agglomeration of the particles that is commonly associated with embedded porosity and poor interfacial bonding plays a significant role in controlling the room temperature strength of the material.

4.3 Theoretical modeling

In this analysis, two parameters are defined to describe particle clustering. They are defined based on volume fraction of particles agglomerated in the cluster and volume fraction of clusters in the matrix. The total volume V_f of particles can be divided into the two following parts:

$$V_f = V_f^c + V_f^m \tag{4.1}$$

where V_f^c is the volume of particles inside a cluster, and V_f^m is the volume of particles in the matrix outside the cluster. Clustering parameters are introduced as follows:

$$\eta = \frac{V_c}{V}, \quad \zeta = \frac{V_f^c}{V_f} \qquad (0 \le \eta, \zeta \le 1) \tag{4.2}$$

where V is volume of composite, V_c volume of clusters, η volume fraction of clusters, ζ volume ratio of the particles inside the clusters over the total particles inside the matrix. These two parameters, η and ζ, can be used to describe the microstructural inhomogeneity of the particulate reinforced composite. In this study, there is an example that explain how to calculate these parameters and use them to interpret clustering defect.

Clustering parameters, η and ζ, are determined based on proposed definition on Eq. (4.2) and using the real microstructure of composite shown in Fig.4.2c for each cluster and then the mean value of these parameters is calculated to show the agglomeration degree of the particles. It should be noted that a cluster is considered as the smallest spherical perimeter region of local agglomerated particles in the microstructure. Clustering parameters, η and ζ, are respectively 0.134 and 0.4897 for this microstructure. This means around 49% of the particles are agglomerated in the clustered regions and the volume fraction of these clustered regions is around 13%.

After defining clustering parameters, a stepping scheme is applied to calculate the effective properties of constituents of composite [Qing-Sheng et. al, 2007]. The cluster is homogenized to obtain an equivalent inclusion, and the same homogenization for the medium containing particles outside the clusters forms an equivalent matrix. Hence, the bulk and the shear modulus of equivalent matrix can be written as below:

$$\kappa_{0,eq} = \kappa_0 \left[1 + \frac{f_1(1-\zeta)(\kappa_1/\kappa_0 - 1)}{1-\eta+\alpha\left[1-\eta-f_1(1-\zeta)\right](\kappa_1/\kappa_0 - 1)} \right]$$
$$\mu_{0,eq} = \mu_0 \left[1 + \frac{f_1(1-\zeta)(\mu_1/\mu_0 - 1)}{1-\eta+\beta\left[1-\eta-f_1(1-\zeta)\right](\mu_1/\mu_0 - 1)} \right] \tag{4.3}$$

and for equivalent inclusion as

$$\kappa_{1,eq} = \kappa_0 \left[1 + \frac{f_1\zeta(\kappa_1/\kappa_0 - 1)}{\eta+\alpha(\eta-f_1\zeta)(\kappa_1/\kappa_0 - 1)} \right]$$
$$\mu_{1,eq} = \mu_0 \left[1 + \frac{f_1\zeta(\mu_1/\mu_0 - 1)}{\eta+\beta(\eta-f_1\zeta)(\mu_1/\mu_0 - 1)} \right] \tag{4.4}$$

where, for spherical inclusions

$$\alpha = \frac{1+\nu_0}{3(1-\nu_0)}, \beta = \frac{2(4-5\nu_0)}{15(1-\nu_0)} \tag{4.5}$$

κ_r and μ_r are the bulk and the shear modulus of the matrix and inclusion (r=0,1).

The Poisson's ratio of the equivalent matrix is given as:

$$\nu_{0,eq} = \frac{3\kappa_{0,eq} - 2\mu_{0,eq}}{6\kappa_{0,eq} + 2\mu_{0,eq}} \tag{4.6}$$

The micromechanical modeling based on Eshelby's equivalence principle incorporated with the Mori-Tanaka's mean field concept is used to calculate the macroscopic stress which leads to initial yielding in the matrix while particle clustering is considered with defined parameters, η and ζ. The mean stress of the matrix and inclusion in the composite system is given by:

$$\sigma^0 = \sigma + \bar{\sigma} = L_0(\varepsilon_0 + \bar{\varepsilon})$$
$$\sigma^1 = \sigma + \bar{\sigma} + \sigma^{pt} = L_1(\varepsilon_0 + \bar{\varepsilon} + \varepsilon^{pt}) = L_0(\varepsilon_0 + \bar{\varepsilon} + \varepsilon^{pt} - \varepsilon^*) \tag{4.7}$$

where ε_0 is the strain of linearly elastic comparison material with matrix subjected to the applied stress. σ and $\bar{\sigma}$ are the applied stress and average stress based on Mori-Tanaka mean field concept, respectively. The subscript 0 refers to the matrix and 1 refers to the inclusions. σ^{pt} and ε^{pt} represent the perturbed parts of stress and the response fields in reinforcements. In this equation, L_1 and L_0 are tangential moduli tensor for the particle and matrix, respectively. In this study, L_1 and L_0 should be substituted into Eq. (4.7) by the equivalent bulk and the shear modulus of the matrix and homogenized cluster region defined in Eqs. (4.3) and (4.4).

After some mathematical manipulations [for details, see Publication 1, 3], the mean stress of the matrix and inclusion in the composite system can be obtained and thus, the hydrostatic and deviatoric components of corresponding stresses can be simplified for equivalent matrix to:

$$\sigma_{kk}^{0} = \frac{\alpha(\kappa_{1,eq} - \kappa_{0,eq}) + \kappa_{0,eq}}{(\eta + (1-\eta)\alpha)(\kappa_{1,eq} - \kappa_{0,eq}) + \kappa_{0,eq}} \sigma_{kk} = a_0 \sigma_{kk}$$
$$\sigma_{ij}^{0\prime} = \frac{\beta(\mu_{1,eq} - \mu_{0,eq}) + \mu_{0,eq}}{(\eta + (1-\eta)\beta)(\mu_{1,eq} - \mu_{0,eq}) + \mu_{0,eq}} \sigma_{ij}' = b_0 \sigma_{ij}' \tag{4.8}$$

and for homogenized cluster region as equivalent inclusion to:

$$\sigma_{kk}^{1} = \frac{\kappa_{1,eq}}{(\eta + (1-\eta)\alpha)(\kappa_{1,eq} - \kappa_{0,eq}) + \kappa_{0,eq}} \sigma_{kk} = a_1 \sigma_{kk}$$
$$\sigma_{ij}^{1\prime} = \frac{\mu_{1,eq}}{(\eta + (1-\eta)\beta)(\mu_{1,eq} - \mu_{0,eq}) + \mu_{0,eq}} \sigma_{ij}' = b_1 \sigma_{ij}' \tag{4.9}$$

Using the definition of macroscopic von Mises equivalent stress and above equations, the initial effective yield stress for the matrix and inclusion is found [for details, see Publication 3]. The matrix will yield at stress is defined as below:

$$\sigma_m = \sigma_{e0} = \frac{\sigma_e^0}{b_0} \tag{4.10}$$

and the homogenized cluster region will yield at the stress

$$\sigma_c = \sigma_{e1} = \frac{\sigma_e^0}{b_1 b_0} \tag{4.11}$$

Under pure tension, σ_e^0 reduces to the ordinary tensile yield stress σ_Y^0.

Figure 4.5 shows the effects of clustering parameters, η and ζ, on the initiation of plastic flow of matrix. Where $\eta = \zeta$, the volume fractions of particles in the cluster and matrix are equal and this implies that all particles are dispersed uniformly in the matrix. Therefore, macroscopic stress for initial yielding normalized by the corresponding value of the matrix, $\sigma_c / \sigma_m \cong 1$. It is seen that with the increase in the relative amount ζ of the particles that are agglomerated in the clusters, σ_c / σ_m increases and plastic flow inside the clusters are more inhibited. For composite with clustering defect, the clustered regions would start yielding at a higher macroscopic stress during uniaxial tension. This implies that, when particles are closely associated with the cluster, the plastic flow on the matrix inside the cluster is constrained and would initiate only after plastic flow begins in the regions without clusters. The decrease in η at constant ζ value means numbers of clustered regions decrease while volume ratio of particles agglomerated in the clusters is constant; therefore, volume fraction

of the particles inside the clusters and rigidity of the clusters increase significantly and σ_c/σ_m increases considerably. In this case, the agglomeration degree of particles is more severe.

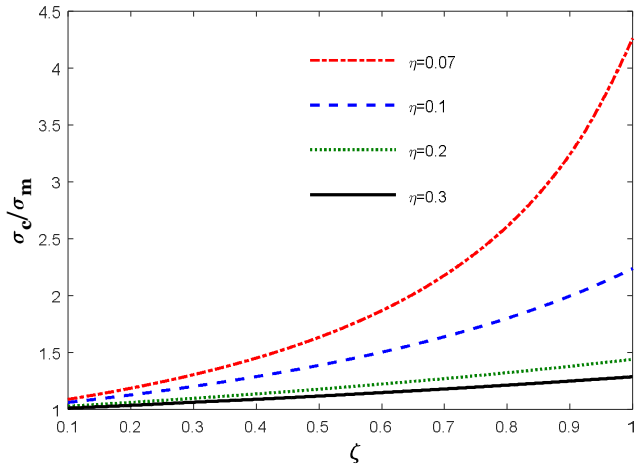

Figure 4.5. Effects of clustering parameters on the initiation of plastic flow of matrix.

4.4 Microstructural modeling

The finite element RVE was created for the micrograph of Fig. 4.1a, thus displaying all microstructural details, i.e., the inclusions with their actual size, shape, spatial positioning, and in the exact amount. Typical RVE with finite element mesh is shown in Fig. 4.6.

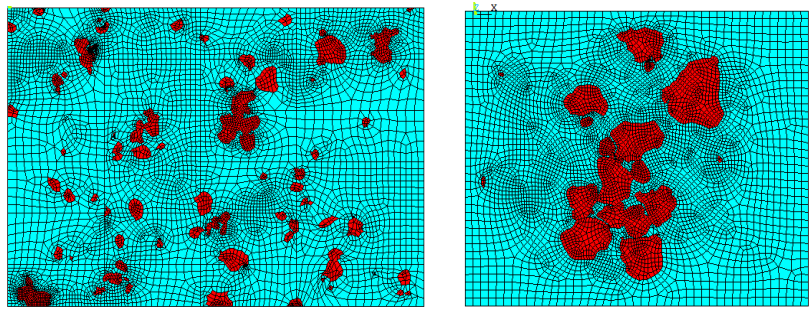

Figure 4.6. RVE and meshing used for finite element modeling.

Figure 4.7a-b depicts von Mises stress distribution and equivalent plastic strain of the typical RVE. Von Mises stress distribution expresses the degree of easiness for plastic deformation. It can be seen that von Mises stress values inside the clustered region are lower than the unclustered region and in some parts of the clustered regions this values is lower than the yield stress of the matrix. These distributions show that the plastic flow on the matrix inside the cluster is constrained and particle clustering has a considerable influence on local plasticity. In other words, crack initiation (debonding and void formation)

at the interface or among the cluster of particles is caused by the constraint of deformation. The constraint of deformation will promote early the void formation in the matrix and interface debonding in the clustering region.

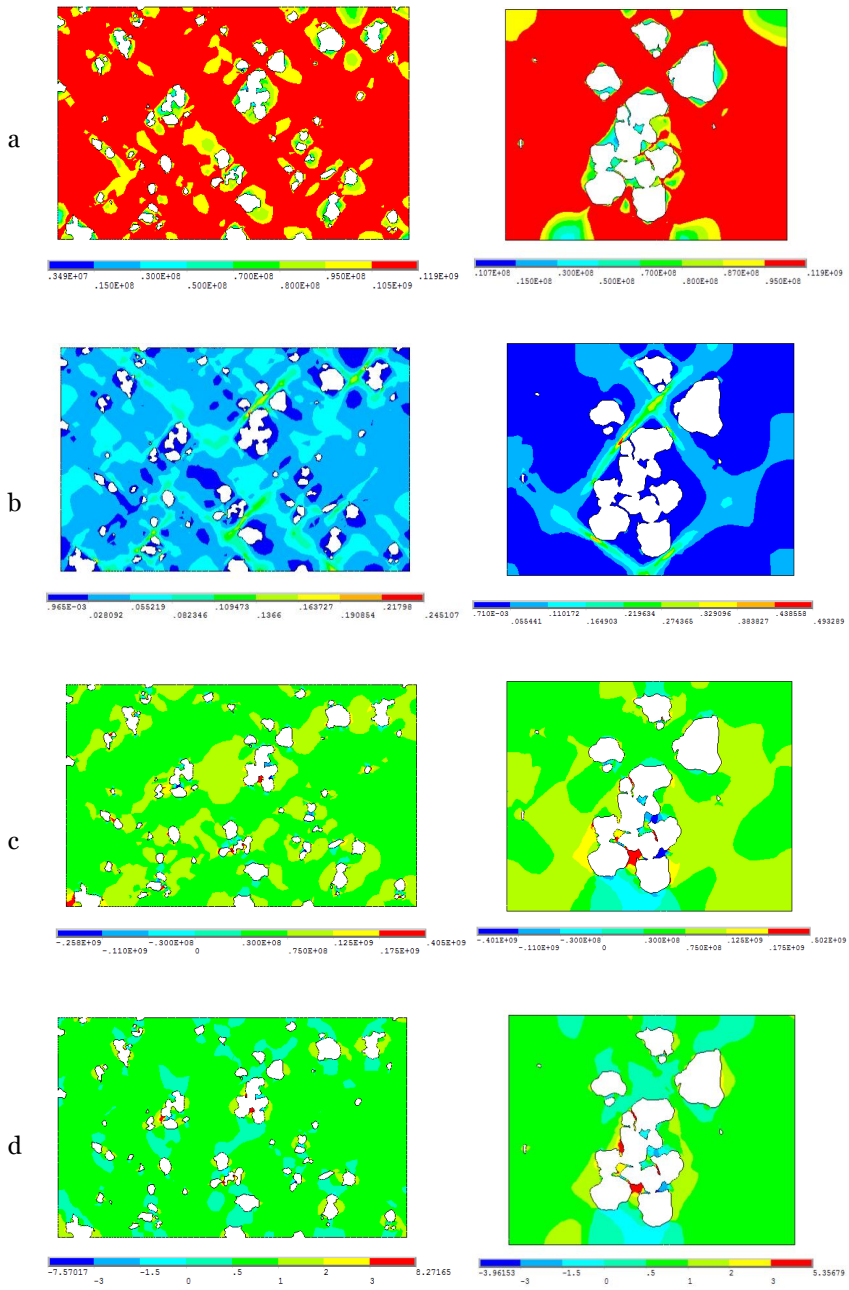

Figure 4.7. (a) von Mises, (b) equivalent plastic strain (c) hydrostatic stress distribution, and (d) stress triaxiality distribution

It is significant to gain a better understanding of the influence of particle clustering on interface debonding and void formation by studying the correlation between von Mises and hydrostatic stress distribution and void formation (crack initiation morphology) of the composite. Figure 4.7c shows the hydrostatic stress of RVE. It can be seen in that the positive and negative peak values of hydrostatic stress which are important factor for debonding and void formation happen in the cluster region. Due to the plastic flow constraint, the hydrostatic stress around the perimeter of a cluster is significantly higher than around an individual particle and, consequently, a greater tendency towards debonding and crack initiation failure mode. Crack initiation morphology is identified from the transverse cross section observation from the fractured specimens during tensile test shown in Figs. 4.4b, 4.5b. It can be seen that interfacial debonding are more prone to occur in the clustered regions and thus there is a good correlation between von Mises and hydrostatic stress distribution and crack initiation morphology. Figure 4.7d shows the effect of particle distribution on stress triaxiality. According to the microscopic mechanism, stress triaxiality describes the advantages of the void mechanism over the shear mechanism during material deformation. When the stress triaxiality is large, void growth is the dominant failure mode. For the low stress triaxiality, a fracture may develop into a combination of the shear and void growth mode.

5. Microstructure effects on fatigue properties and crack growth mechanism

5.1 General marks

In automotive and aerospace industries, composites should sustain mechanical loading. Thus, the resistance of amorphous particulate reinforced composites as a new class of materials to fatigue crack growth must be explored prior to their application in industries. The high cycle fatigue properties and crack propagation mechanism of Mg-amorphous alloy composite have not yet been clarified in details. This study investigates high cycle fatigue properties and crack propagation mechanism of novel Mg-amorphous alloy composite. Moreover, the effect of particle distribution and morphology on fatigue behavior and crack growth process is studied. Since the composites are fabricated by a powder metallurgy and extrusion process, it is often difficult to obtain a uniform and homogeneous distribution of reinforcement particles practically. A detailed understanding of fatigue failure processes is, therefore, of considerable interest to reliably predict and optimize the fatigue resistance of these materials.

5.2 Experimental details

The new class of Mg-composite reinforced with amorphous alloy particles is fabricated by a powder metallurgy and extrusion process as explained in previous chapter, section 4.2. The extruded rods were used for further testing and fatigue tests were conducted on hour-glass shaped round specimens; the dimensions of the specimens are shown in Fig. 5.1. After machining, a layer with thickness of about 100 μm was removed from the surface of the specimens by electrolytically polishing in order to avoid the influence of machining on the fatigue results.

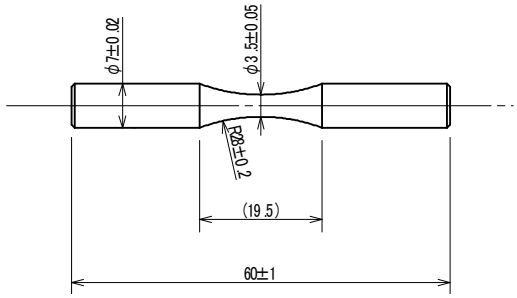

Figure 5.1. Configuration of fatigue specimen.

The microstructures of $Ni_{60}Nb_{40}$/Mg composites with varying volume fractions, particles distribution and extrusion loads are depicted in Fig. 5.2a-d. The results of tensile testing and microstructural characterization clearly reveal that the distribution of reinforcement particles controls the extrusion load [Publication 3].

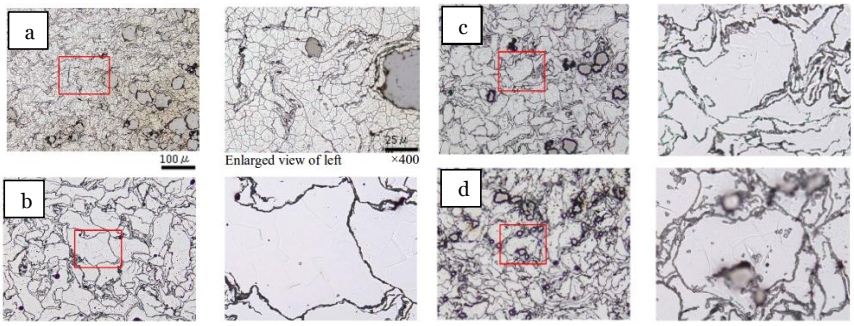

Figure 5.2. Microstructure of composites: (a) 5 vol. % composite 750 psi, (b) 600 psi, and (c) 3 vol. % composite 650 psi, (d) 3 vol. % composite 550 psi.

5.3 Results and discussion

5.3.1 Fatigue strength

To study particle distribution and morphology effect on fatigue strength, the S–N curves of 3 and 5 vol. % composite were shown for specimens chosen from billets extruded at different pressure. Fatigue strength data were obtained at a stress ratio, $R = -1$, and a frequency of 20 Hz in laboratory air at ambient temperature.

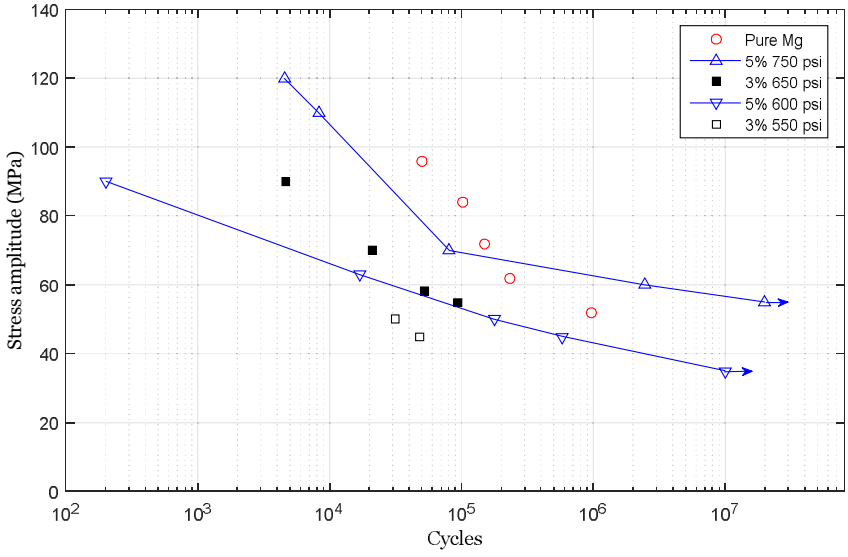

Figure 5.3. *S-N* curves of different composition of $Ni_{60}Nb_{40}$/Mg composite.

Figure 5.3 shows the S–N curves for specimens with varying volume fractions (3% and 5%) of particles and pure magnesium. The distinction of the S–N curves between these specimens should be ascribed to the different microstructures. The specimen with more uniform particle distribution possesses a superior fatigue resistance in fatigue limit. It can be also seen the fatigue life of amorphous particulate reinforced composite is higher than that of pure Magnesium in high cycle region.

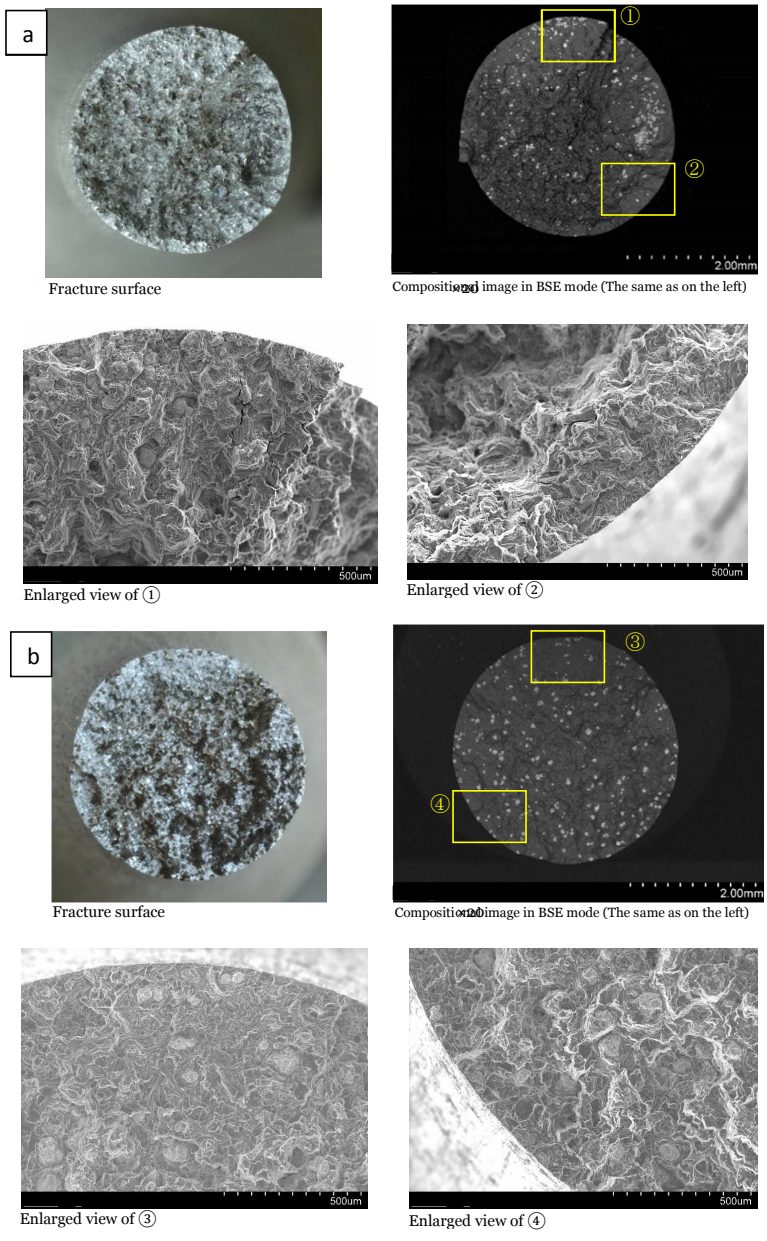

Figure 5.4. Fracture surface observations of 3 vol. % composite extruded at: (a) 550 psi and (b) 650 psi

Examples of fracture surface observations of the specimens with different particles distribution for 3 and 5 vol. % composite are shown in Figs. 5.4 and 5.5, respectively. It can be seen there are several fracture origions in the case of non uniform particles distribution and these conditions influenced fatigue life of the material.

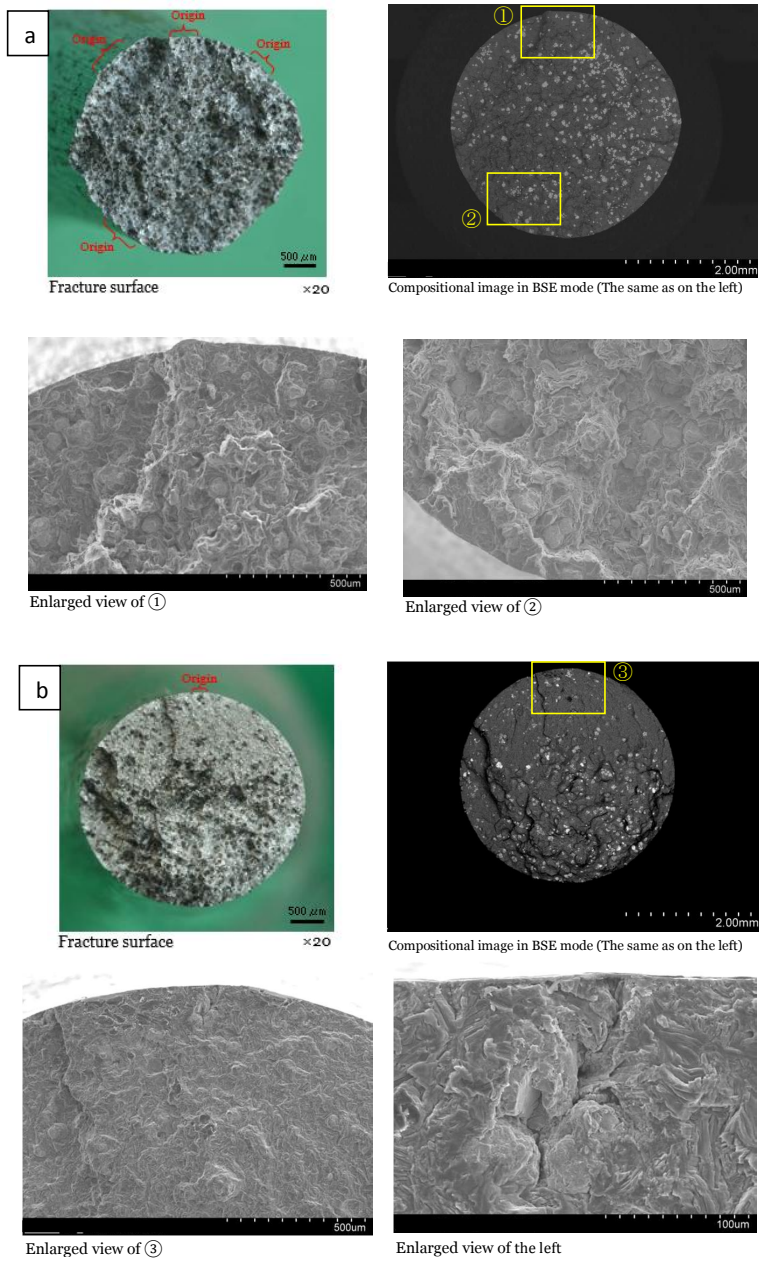

Figure 5.5. Fracture surface observations of 5 vol. % composite extruded at: (a) 600 psi and (b) 750 psi

5.3.2 *In situ* observations of crack growth behavior

The crack initiation and propagation behavior during the fatigue process were monitored with replication technique. Fatigue testing was periodically interrupted at fixed numbers of cycles and replicas were taken and then crack length was measured using a laser microscope. In this technic, a thin acetate film is softened with solvent and applied to the curved surface of the specimen, then film is dried and can be removed. This film can be maintained permanently to observe crack morphology.

In situ observation of crack growth process at constant stress amplitude was carried out for different 3% and 5% volume fractions of particles to observe fatigue crack initiation and propagation of amorphous particulate reinforced composites. Figures 5.6 and 5.7 show the successive observations of the specimen surface during the fatigue process of 3% and 5% volume fractions of $Ni_{60}Nb_{40}$ particles at stress amplitude 55 and 70 MPa, respectively.

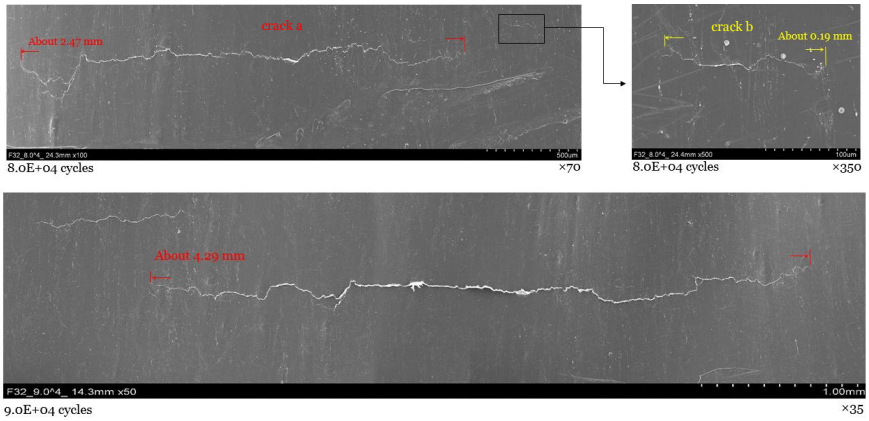

Figure 5.6. *In situ* observation of the specimen surface of 3 vol. % composites (extrusion pressure 650 psi) during fatigue process.

As seen from Fig. 5.7, multiple cracks that initiated at the interface between $Ni_{60}Nb_{40}$ particles and matrix propagated when short in isolation, with no interaction between them. However, the multiple cracks coalesced with each other when they propagated further and cracks grew by repletion of coalesce. These observations showed when the crack tip reached adjacent $Ni_{60}Nb_{40}$ particle, the crack runs around the particle-matrix interface and then propagate through the matrix. It can be seen there is no fracture of particles at the crack front.

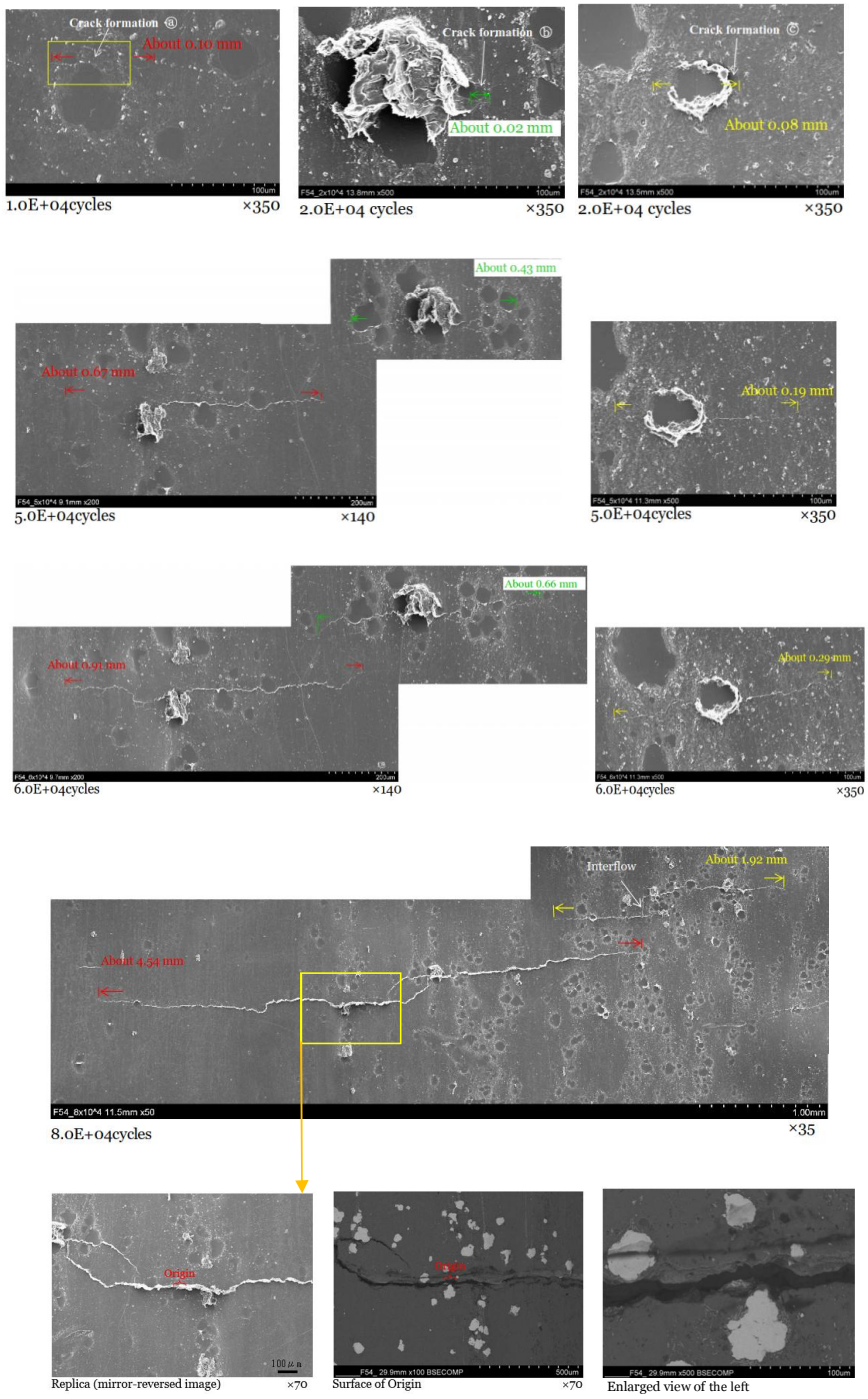

Figure 5.7. *In situ* observation of cracks initiation and propagation of 5 vol. % composites with more uniform distribution (extrusion pressure 750 psi) during fatigue process.

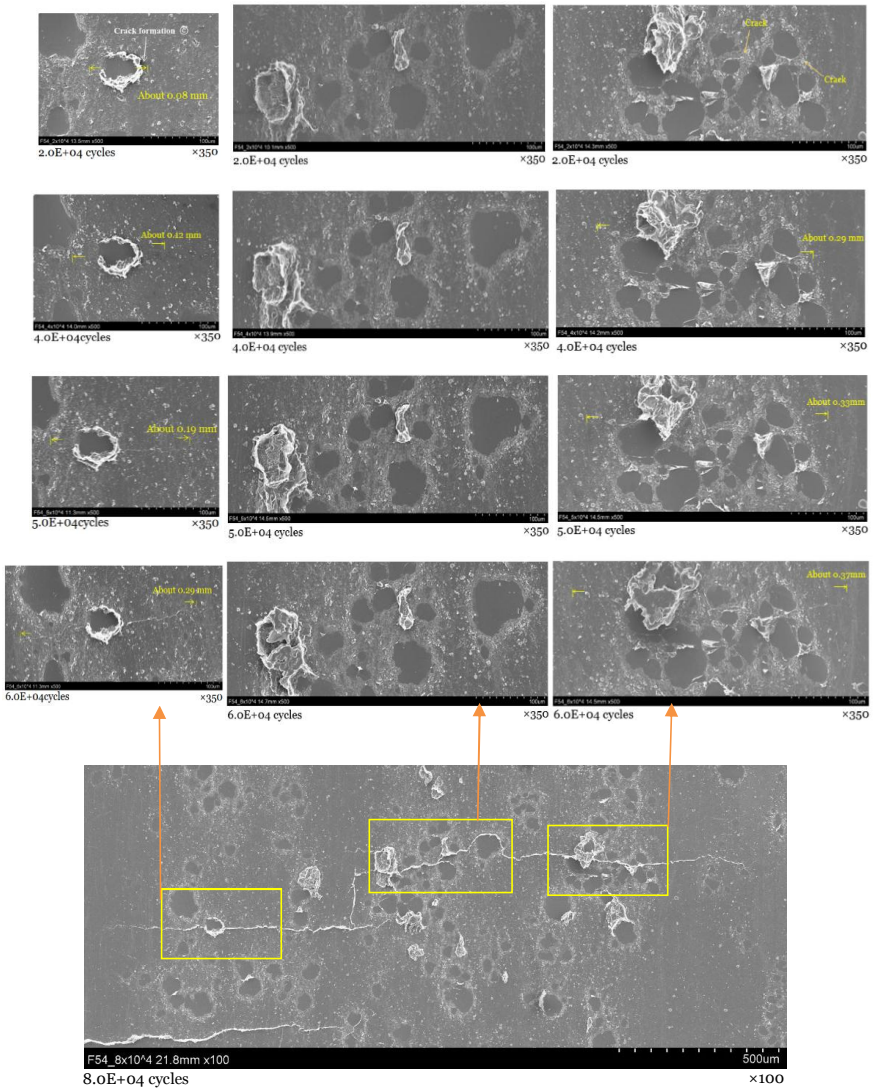

Figure 5.8. *In situ* observation of crack initiation and propagation in clustered region (5 vol. % composites, $\sigma_a = 70MPa$).

To investigate the localized damage of present amorphous particulate reinforced composite, more detailed *in situ* observation of crack initiation and growth mechanism was carried out. Figure 5.8 shows an example of *in situ* crack initiation and propagation in clustered region. As seen from the figure, multiple cracks initiated at the particle-matrix interfaces and the matrix itself and following some cycles, the micro-cracks coalesce to become a main crack. The crack growth rate of the main crack initiated from clustered region is high.

The successive microstructural observations of the specimen surface of 5 vol. % composite in high cycle region ($\sigma_a = 55MPa$) are depicted in Fig. 5.9. Small crack was observed at the interface of $Ni_{60}Nb_{40}$ particle using SEM. With increasing number of cycles, crack propagation is very low but likely the crack is non-propagating ($dl / dN \cong 0$). It can be seen that particle is fractured with increasing number of cycles. The fracture of particles plays a key role in sustaining crack growth in high cycle region.

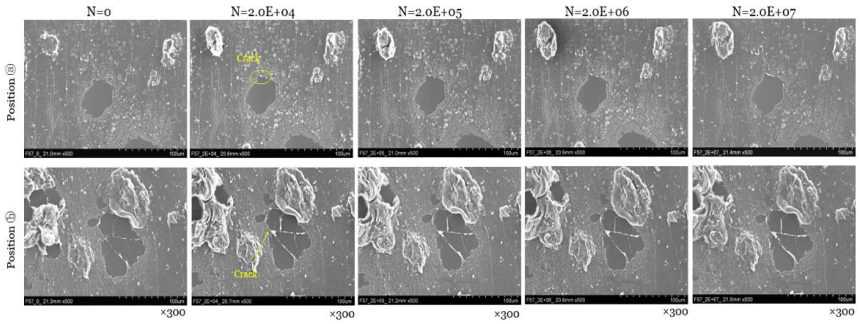

Figure 5.9. *In situ* observation of the specimen surface in high cycle region.

In addition, *in situ* observation of specimen with non-uniform distribution of 5 vol. % composite at stress amplitude 63 MPa is depicted in Fig. 5.10. This specimen is chosen from the billet with extrusion pressure 600 psi. Many cracks were observed by replica method in this figure. It can be seen that crack coalescence occurs by the initiation of multiple cracks during fatigue test for non-uniform distribution of particles while in the case of uniformly distributed particles, crack coalescence did not readily occur, since crack initiation was limited. The difference of the microstructure is the cause for different crack initiation and propagation and this condition influenced fatigue life as shown in Fig. 5.3.

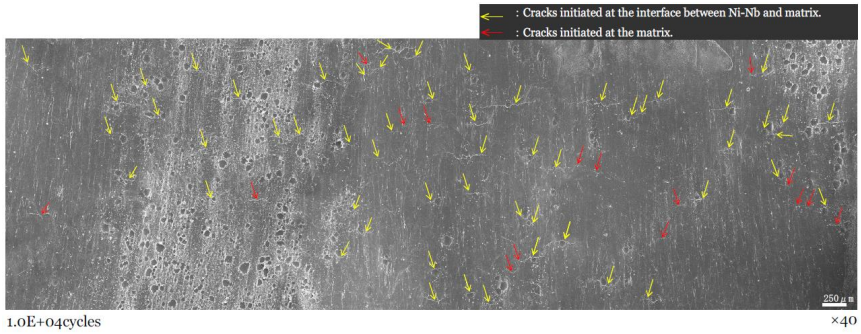

Figure 5.10. *In situ* observation of specimen with non-uniform distribution of 5 vol. % composites at stress amplitude 63 MPa.

5.3.3 Crack propagation behavior

As a damage process, fatigue is traditionally divided into a crack initiation phase and a crack propagation phase. In the case of amorphous particulate reinforced composite examined in the current study, the latter process is more important because most fatigue life is spent by the propagation life of cracks, especially small cracks. Therefore, it is very important to clarify the crack mechanism and examine models which can assist in fatigue life prediction.

Figure 5.11 shows the variations of crack length l measured from successive observations as a function of number of cycles N for 3% volume fraction composite at a stress amplitude 55 MPa and 5% volume fraction composite at a stress amplitude 70 MPa. Coalescence of cracks occurred at positions C in the figure. For 5% volume fraction, it can be seen that a crack initiated at about 12% of the fatigue life and coalesced with another crack at about 75% of the fatigue life. On the other hand, for a 3% volume fraction sample, a crack initiated at 20% of the fatigue life and coalesced with another crack at 85% of the fatigue life.

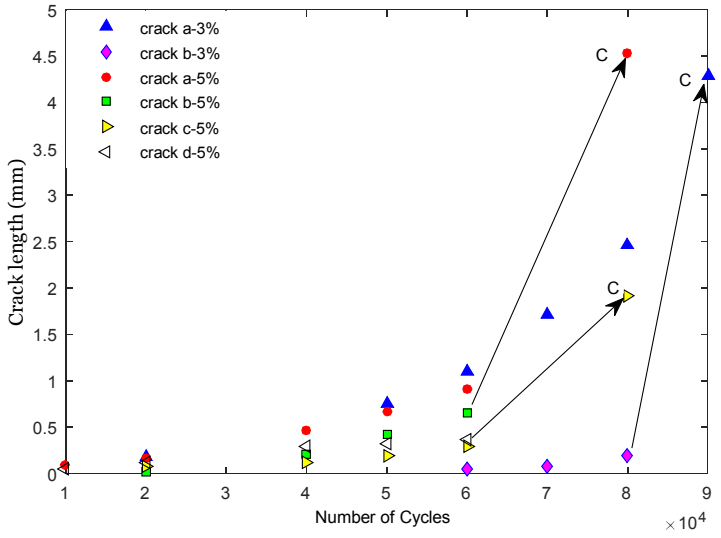

Figure 5.11. Variations of crack length as a function of number of cycles.

The relationship between the rate of the crack growth, dl/dN, and crack length, l, is considered as below [Nisitani et. al, 1994]:

$$dl/dN = C\sigma_a{}^n l \tag{5.1}$$

where σ_a is the stress amplitude, and C, n are constants. This equation is correlated with data presented in Fig. 5.10 and it can be used for crack propagation through the matrix and region of well dispersed particles. In order to derive the crack length relation from the crack growth law, Eq. (5.1), this equation is integrated to obtain:

$$l = l_o \exp[C\sigma_a{}^n (\mathrm{N} - \mathrm{N}_o)] \tag{5.2}$$

where l_o represents the initial surface crack length at the number of stress cycles N_o.

Crack growth rates for surface cracks of 5% volume fraction composite specimen fatigue tested at stress amplitude 70 MPa are shown as a function of crack length in Fig. 5.12. This figure shows two examples of the growth behavior of the surface cracks, (1) the crack propagated through the matrix and region of well-dispersed particles (cracks a and c in Fig. 5.7) and (2) the crack encountered a region of clustered particles in its path (crack b in Fig. 5.7).

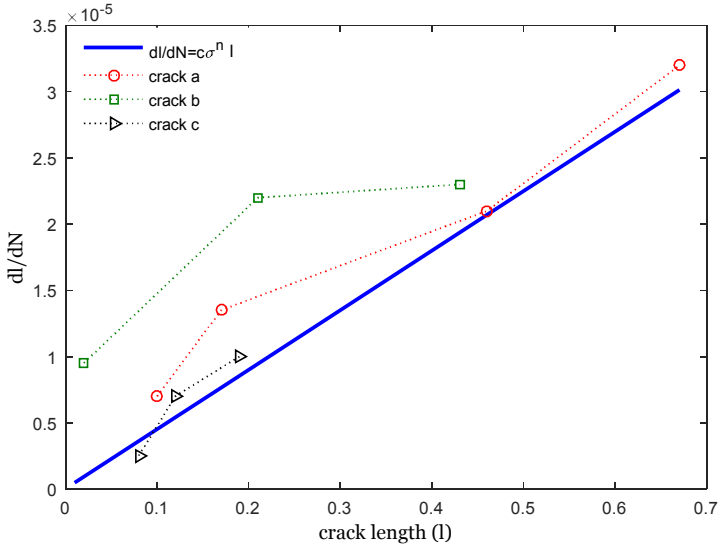

Figure 5.12. Crack growth rates as a function of crack length.

It can be seen that the rate of the crack growth is nearly constant and significantly greater than predicted by the Eq. (5.1) when crack propagates through the clustered region. This trend is different from that of crack propagation through the matrix and region of well-dispersed particles. The effect of particle distribution on crack growth is quantified by tortuosity of the crack path. Tortuosity is defined as the ratio of total crack length divided by the projected crack length. It was observed that tortuosity for crack paths (a) and (b) are 1.14 and 1.34, respectively. Greater tortuosity implies higher local crack resistance, and thus the local constant crack growth rate in a region of particle clusters is due to greater tortuosity in this region, e.g., see Fig. 5.7.

Figure 5.13 shows measured crack length vs. number of fatigue cycles for two samples with 3% and 5% volume fractions. In addition, the crack lengths from Eq. (5.2) for these tests are also shown. Small difference in the constants C and n are observed for the two materials, but, generally speaking, the crack propagation behavior through the magnesium matrix was the same for both materials. This equation is considered to be suitable for modelling crack propagation through the matrix and through regions of well-dispersed particles. However, it does not model the coalescence of cracks which was also observed to occur. It can be seen in Fig. 5.13 that for the 5% volume fraction specimen that the actual

crack length at 8×10^4 cycles was about 4.6 mm which was about twice as long as would be predicted by the Eq. (5.2), see point A and B in Fig. 5.13. This was due to the coalescence of a single crack propagating through matrix with another crack propagating through a region of particle clusters.

In the case of the 3% volume fraction specimen, there was only a single crack which propagates according to Eq. (5.2) for 9×10^4 cycles before coalescing with a much smaller (0.33 mm) crack. Thus, crack propagation of a single crack which then coalesces with small cracks in a region of well-dispersed particles is significantly different from crack propagation of a single crack coalescing with cracks propagating through a region of particle clusters. Results obtained from this figure and *in situ* observations imply that the crack growth in particle reinforced composite is highly localized phenomenon.

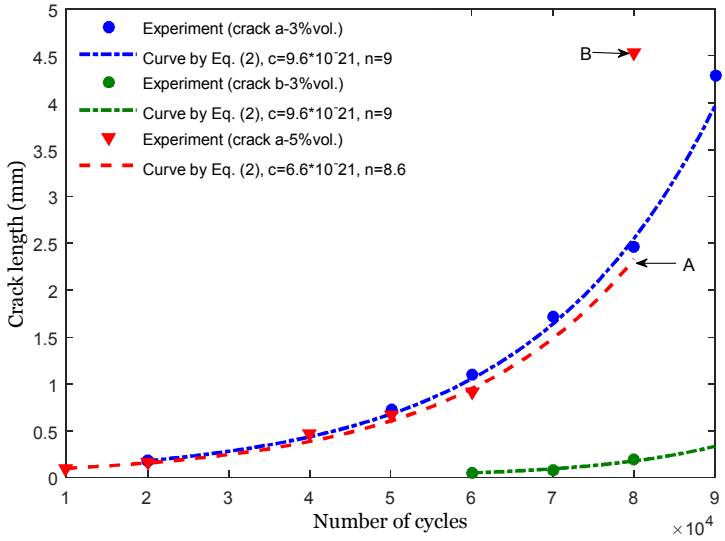

Figure 5.13. Relation between crack length and relative number of cycles.

6. Conclusions

6.1 Summary and conclusion

In order to predict and optimize the mechanical properties of composites, real engineering situations and appropriate assumptions should be considered. The present study was conducted to investigate the debonding damage and particle distribution effects of reinforcements on effective mechanical properties of particulate reinforced composites using theoretical and numerical methodology.

A micromechanical model is developed to take into account debonding of reinforcements, particle size and as well as the elastoplasticity by means of incremental damage theory. The results show that when the debonding damage starts to occur and the volume fraction of debonded particles increases, the stress-strain curve for the damaged nanocomposite deviate to lower stress from those for the perfect composite. The influences of adhesive energy, γ, at interface and particle size, a, are considerable on the stress-strain curve. In the case of a lower γ and larger a value, the stress-strain relation of damaged composite deviate from that of the perfect composite at a lower stress level. When the particle size decreases and the adhesive energy at interface increases, the volume fraction of perfectly bonded particles increases and the volume fraction of debonded particles decreases.

To characterize and gain a better insight into reinforcement/matrix interfacial debonding phenomena, a cohesive finite element method is proposed. The CZM has been adoted to capture reinforcements debonding. When implemented in the FEM, the CZM is capable of simulating interface debonding and sliding. In this study, a computational tool able to map a composite microstructure onto a finite element mesh is adopted to construct models which reproduce the composite microstructure and characteristics. The results show that the assumption of fully bonded particles in composites under loading is incomplete and the influence of cohesive energy, γ_c, at interface is considerable. In the case of a lower γ_c value, the potential sites for debonding are more.

The void initiation and growth or decohesion between the reinforcements and matrix takes place at higher strained region. Therefore, strain localization zone (shear band) can be considered as a zone which is highly potential sites for void initiation. The results indicate that the modeling based on array distribution assumption can not accurately predict the damage behavior and potential sites for debonding and damage initiation of particulate reinforced composites while the modeling based on real microstructure mapping has such ability.

In order to study effects of particle clustering on mechanical properties, damage initiation and plastic deformation of particulate reinforced composites, a new micromechanical modeling is presented. The microstructural inhomogeneity is described in this model by defining two parameters based on volume ratio of particles inside clusters and volume fraction of clusters inside the matrix. The results indicate that the plastic flow on the matrix inside the cluster would initiate only after plastic flow begins in the regions without clusters. Based on the proposed clustering parameters, clustering defect will have minimum effect when volume fraction of clusters increases while the volume fraction of particles agglomerated inside the clusters decreases.

To gain a deeper understanding into clustering defect on plastic deformation and damage initiation, a simulation methodology based on finite element method are developed. In this study, clustering is not based on randomly generated artificial microstructure, but it has been discussed considering real morphology of particles with their actual size, shape, spatial positioning, and in the exact amount. The FEM simulation shows that the plastic flow on the matrix inside the cluster is inhibited. Due to the plastic flow constraint, there is a great tendency towards debonding and crack initiation around the perimeter of a cluster. Following the model validation, experimental observation from the transverse cross-section of fractured specimen shows that the constraint of deformation will promote early the void formation in the matrix and interface debonding in the clustering region and there is a strong relationship between damage formation and the local volume fraction of reinforcements.

Moreover, effects of microstructure and particle clustering on fatigue properties and crack initiation and propagation of novel amorphous particles reinforced Mg-composites are investigated. The experimental results indicate that fatigue properties of particulate reinforced composites depend upon the microstructure and particle distribution. It can be concluded that composites with more uniform particle distribution possess a superior fatigue resistance and fatigue limit.

In situ observations of fatigue crack growth clarify that for non-uniformly distributed particles, crack coalescence of many cracks occurred. By contrast, for more evenly distributed particles, fewer fatigue cracks initiated and crack coalescence did not readily occur. In this case, fatigue was dominated by the propagation of individual fatigue cracks. The difference of the microstructure is the cause for different crack initiation and propagation and this condition influenced fatigue life.

The results show that the crack growth in particulate reinforced composites is a highly localized phenomenon influenced primarily by the distribution and microstructure of particles near the vicinity of the crack tip. The rate of the crack growth through the clustered region was significantly higher than through the matrix or through a region of well-dispersed particles.

6.2 Future developments

In the present study, the mechanical properties of particulate reinforced composites based on appropriate assumptions and real engineering situations is predicted by means of analytical and computational methods. Moreover, effects

of real morghology and spatial distribution of particles on mechanical properties, failure mechanism and fatigue behavior of novel lightweight metal composites reinforced with amorphous particles have been studied. A modelling approach closely related to the real microstructure of composites is proposed. The SEM and TEM micrographs are used to create the finite element 2D RVE displaying all microstructural details, i.e., the inclusions with their actual size, shape, spatial positioning and in the exact amount.

The finite element simulation in this study can be further improved in future by using 3D Images from micro or nano tomography; however, there are modeling complexities and computational difficulties. This kind of studies based on real morphology and microstructure of materials and not based on randomly generated artificial microstructure is essential in the development and design of materials to further applications in real engineering situations.

References

Ayyar, A., Crawford, G.A., Williams, J.J., Chawla, N. (2008). Numerical simulation of the effect of particle spatial distribution and strength on tensile behavior of particle reinforced composites. Comput. Mater. Sci; 44:496–506.

Borbely, A., Biermann, H., Hartmann, O. (2001). FE investigation of the effect of particle distribution on the uniaxial stress–strain behaviour of particulate reinforced metal-matrix composites. Mater. Sci. Eng. A; 313:34–45.

Boutaleb, S., Zairi, F., Mesbah, A.N., Abdelaziz, M., Gloaguen, J.M., Boukharouba, T. (2009). Micromechanics-based modelling of stiffness and yield stress for silica/ polymer nanocomposites. Int J Soli Struct; 46: 1716-26.

Cantwell, W.J., Roulin-Moloney, A.C., (1989). Fractography and failure mechanisms of unfilled and particulate filled epoxy resins. In: Fractography and Failure Mechanisms of Unfilled and Particulate Filled Epoxy Resins; 234–289.

Chen, J.K., Wang, G.T., Yu, Z.Z., Huang, Z., Mai, Y.W., (2010). Critical particle size for interfacial debonding in polymer/nanoparticle composites. Compos. Sci. Tech; 70:861–72.

Conlon, K.T., Wilkinso, D.S., (2001). Effect of particle distribution on deformation and damage of two-phase alloys. Mater. Sci. Eng. A; 317:108–114.

Deng, X., Chawla, N., (2006). Modeling the effect of particle clustering on the mechanical behavior of SiC particle reinforced Al matrix composites. J. Mater. Sci; 41:5731–5734.

Eshelby, J.D., (1957). The determination of the Elastic Field of an Ellipsoidal Inclusion, and Related Problems. Proc Royal Society London; 241 (A): 376-396.

Gent, A.N., (1980). Detachment of an elastic matrix from a rigid spherical inclusion. J. Mater. Sci; 15(11):2884–8.

Nisitani, H., Kawagoishi, N., Goto, M., (1994). Growth behavior of small fatigue cracks and relating problems, in: A. Carpinteri (Eds.), Handbook of fatigue crack propagation in metallic structures, Elsevier science B.V., Netherlands, pp. 733-778.

Habibnejad-Korayem, M., Mahmudi, R., Poole, W.J., (2009). Enhanced properties of Mg-based nanocomposites reinforced with Al_2O_3 nanoparticles. Mater Sci and Eng A; 519:198-203.

Hong, S.J., Kim, H.M, Huh, D., Suryanarayana, C., Chun, B.S., (2003). Effect of clustering on the mechanical properties of SiC particulate-reinforced aluminum alloy 2024 metal matrix composites. Mater. Sci.and Eng. A; 347:198–204.

Koyama, S., Katano, S., Saiki, I., Iwakuam, T., (2011). A modification of the Mori–Tanaka estimate of average elastoplastic behavior of composites and polycrystals with interfacial debonding. Mech. Mater; 43: 538–555.

Kumai, S., Hu J., Higo, Y., Nunomura, S., (1996). Effect of dendrite cell size and particle distribution on the near-threshold fatigue crack growth behavior of cast Al-SiCp composites. Acta. Mater; 44: 2249–57.

Lauke, B., Schuller, T., Beckert, W., (2000). Calculation of adhesion strength at the interface of a coated particle embedded within matrix under multiaxial load. Comput. Mater. Sci; 18:262–380.

Lauke, B., (2013). Effect of particle size distribution on debonding energy and crack resistance of polymer composites. Comput. Mater. Sci; 77: 53-60.

Lewandowski, J.J., Liu, C., Hunt, W.H., (1989). Effects of matrix microstructure and particle distribution on fracture of an aluminum metal matrix composite. Mater. Sci. Eng. A; 107:241–255.

Li, M., Ghosh, S., Richmond, O., (1999). An experimental–computational approach to the investigation of damage evolution in discontinuously reinforced aluminum matrix composite. Acta. Mater; 47:3515–32.

Lorca, J., (2002). Fatigue of particle and whisker- reinforced metal matrix composite. Prog. Mater. Sci; 47:283-353.

Mishnaevsky, L., Derrien, K., Baptiste, D., (2004). Effect of microstructure of particle reinforced composites on the damage evolution: probabilistic and numerical analysis. Compos. Sci. Technol; 64:1805–1818.

Mori, T., Tanaka, K., (1973). Average stress in matrix and average elastic energy of materials with misfitting inclusions. Acta. Metall; 21:571–4.

Mura, T., (1987). Micromechanics of defects in solids. 2nd edition. New York: Martins Nijhoff.

Murphy, A.M., Howard, S.J., Clyne, T.W., (1998). Characterisation of severity of particle clustering and its effect on fracture of particulate MMCs. Mater. Sci. Techno; 14:959–68.

Needleman, A., Xu, X.P., (1994). Numerical simulation of crack growth in brittle solids, J. Mechan. Phys. Solids; 42: 1397-1434.

Nicholson, D.W., (1979). On the detachment of a rigid inclusion from an elastic matrix. J. Adhes; 10:255–60.

Odegard, G.M., Clancy, T.C., Gates, T.S., (2005). Modeling of mechanical properties of nanoparticle/polymer composites. Polymer; 46: 553-62.

Qing-Sheng, Y., Xu, T., Hui, Y., (2007). A stepping scheme for predicting effective properties of multi-inclusion composites. Int. J. Eng. Sci; 45:997–1006.

Salviato, M., Zappalorto, M., Quaresimin, M., (2013). Nanoparticle debonding strength: A comprehensive study on interfacial effects. Int. J. Solids. Struct; 50: 3225–3232.

Segurado, J., Gonzalez, C., Llorca, J., (2003). A numerical investigation of the effect of particle clustering on the mechanical properties of composites. Acta. Mater; 51: 2355–2369.

Segurado, J., Llorca, J., (2006). Computational micromechanics of composites: The effect of particle spatial distribution. Mech. Mater; 38:873–883.

Shao, L.H., Luo, R.Y., Bai, S.L., Wang, J., (2009). Prediction of effective moduli of carbon nanotube–reinforced composites with waviness and debonding. Compos. Struc; 87: 274–81.

Singh, H., Mao, Y., Sreeranganathan, A., Gokhale, A.M., (2006). Application of digital image processing for implementation of complex realistic particle shapes/morphologies in computer simulated heterogeneous microstructures. Model. Simul. Mater. Sci. Eng; 14:351–363.

Tohgo, K., Weng, G.J., (1994). A progressive damage mechanics in particle-reinforced metal-matrix composites under high triaxial tension. ASME 1 Eng. Mat.Tech; 116:414-420.

Zappalorto, M., Salviato, M., Quaresimin, M., (2011). Influence of the interphase zone on the nanoparticle debonding stress. Compos. Sci.Technol; 72:49-55.

Errata

Publication	Place	Instead of	Read
[P1]	Fig. 2	$a = 8nm$	$a = 50nm$
[P1]	Eq. (3)	$d\sigma_3^{pt}$	σ_3^{pt}
[P1]	Eq. (6)	ε_3^{pt}	σ_3^{pt}
[P2]	Fig. 8	[MPa]	should be omitted

To predict and optimize the mechanical properties of new class of advanced composites, real engineering situations and appropriate assumptions should be considered. Moreover, a profound understanding of the relationship between real microstructure of composites and their mechanical properties is necessary. This study is concerned with the debonding damage and particle distribution effects of reinforcements on overall mechanical properties of particulate reinforced light weight metal matrix composites. The results show that the assumption of fully bonded particles in composites under loading is incomplete and the influence of cohesive energy at interface is considerable. Findings show there is a strong relationship between damage formation and the local volume fraction of reinforcements. The crack growth in particulate reinforced composites is a highly localized phenomenon influenced primarily by the distribution and microstructure of particles near the vicinity of the crack tip and thus the assumption of uniform distribution is inadequate.

Aalto-DD 173/2016

ISBN 978-952-60-6990-6 (printed)
ISBN 978-952-60-6989-0 (pdf)
ISSN-L 1799-4934
ISSN 1799-4934 (printed)
ISSN 1799-4942 (pdf)

Aalto University
School of Engineering
Department of Mechanical Engineering
www.aalto.fi

BUSINESS + ECONOMY

ART + DESIGN + ARCHITECTURE

SCIENCE + TECHNOLOGY

CROSSOVER

DOCTORAL DISSERTATIONS